Microfluidic cancer cell sorting using dielectrophoresis

Master's thesis, 1.7.2020

Author:

Peter Balogh

Supervisor:

Andreas Johansson

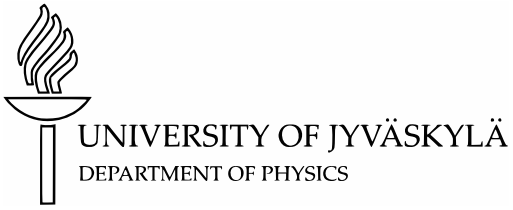

UNIVERSITY OF JYVÄSKYLÄ
DEPARTMENT OF PHYSICS

Abstract

Balogh Peter

Microfluidic cancer cell sorting using dielectrophoresis

Master's Thesis

Department of Physics, University of Jyväskylä, 2020, 74 pages

Microfluidics grant the possibility for the analysis of microbiological particles such as cells, viruses, proteins, and DNA. It can fulfil the strict requirements for temperature, pressure, and chemical composition set by samples in vivo environment. The aim was to develop the fabrication of a microfluidic chip that would be capable of single cell sorting, fluorescently labelled cancer cells to be more precise. Cells flowing through the system would be analysed using spectroscopy to detect fluorescence. Depending on the result, a dielectrophoretic force would be exerted on the target cell guiding it to a corresponding channel to be collected or discarded. Achieving a high throughput device that could analyse thousands of cells a second while sorting individual cancer cells from blood samples would have a significant impact on cancer research.

Glass, being transparent and chemically inert, is an optimal material for spectroscopic analysis and as a microfluidic environment. Thus, a fabrication recipe for a glass (Soda-lime) microfluidic chip including electrodes was developed. Using electron beam lithography and thin film deposition, such a chip was realised with minimised defects. The electrodes consisted of a sandwich of Ti, Au, Ti and SiO_2. They could withstand the highly corrosive Piranha treatment for surface activation and the temperature of 585 °C required for the glass bonding. The cleaning procedure of the chip, etch mask, and etching parameters were optimized to minimize pinhole generation and channel roughness. As an etch mask, thin film layers of 50 nm Cr and 200 nm + 100 nm Au were used. It enabled a near defect free etching of 30 µm deep channels in HF while protecting the underlining electrodes. An experimental setup was assembled to demonstrate deflection of fluorescent polystyrene particles illustrating cells. The proper flow of fluorescent particles was established, but the sorting was unsuccessful most likely due to a faulty electrode. The fabrication of a new chip was unfortunately not possible because of the facility lockdown due to the covid-19 pandemic. However, the fabrication recipe and design improvement ideas presented here grant a good foundation for future continuations on this project.

Keywords: Glass microfluidics, Wet etching of glass, Dielectrophoresis (DEP), Cell sorting, Fabrication

Tiivistelmä

Peter Balogh

Syöpäsolujen erottelu dielektroforeesilla mikrofluidisessa ympäristössä

Pro gradu -tutkielma

Fysiikan laitos, Jyväskylän yliopisto, 2020, 74 pages.

Mikrofluidiikka mahdollistaa mikrobiologisten partikkeleiden, kuten solujen, viruksien, proteiinien ja DNA:n analysoinnin. Se pystyy täyttämään näiden tiukat elinolojen vaatimukset, joita ovat paine, lämpötila ja kemiallinen koostumus. Tarkoituksena oli kehittää valmistusmenetelmä mikrofluidiselle sirulle, joka pystyisi erottelemaan yksittäisiä fluoresenssilla merkattuja syöpäsoluja. Sirussa kulkevia soluja tarkasteltaisiin spektroskopian menetelmin, ja mikäli solu ilmaisisi fluoresenssia, dielektroforeesinen voima ohjaisi sen erilleen talteen otettavaksi. Valmistamalla tällainen siru, joka pystyisi analysoimaan verinäytteestä tuhansia soluja sekunnissa ja erottelemaan niistä yksittäiset syöpäsolut, pystyttäisiin vaikuttamaan merkittävästi syöpätutkimuken kehitykseen.

Lasi on optimaalinen valinta tällaiselle sirulle, sillä sen läpinäkyvyys ja kemiallinen vakaus mahdollistvat spektroskopian ja mikrofluidisen ympäristön tarjoamisen. Tästä syystä siru oli kehitetty käyttämällä substraattina soda-lime lasia. Käyttämällä elektronisuihkulitografiaa, fysikaalista kalvonkasvatusmenetelmää sekä muita mikrofabrikaation työkaluja, siru saatiin valmistettua. Dielektroforeesia varten valmistettiin elektrodit, jotka koostuivat Ti, Au ,Ti ja SiO_2 kerroksista. Ne olivat tarpeeksi kestäviä selvitääkseen lasien bondaukseen tarvittavasta korkeasta lämpötilasta (585 °C) sekä hyvin syövyttävästä Piranha liuoksesta. Sirun puhdistusmenetelmät, etsausmaski sekä etsausparametrit optimoitiin tasaisen ja virheettömän pinnan aikaansaamiseksi. Etsausmaskina käytettiin 50 nm Cr ja 200 nm + 100 nm Au, joka kesti 30 µm syvien kanavien etsauksen vetyfluoridilla ja pystyi suojelemaan sen alla olevia elektrodeja. Koejärjestely suoritettiin dielektroforeettisen erottelun havainnollistamiseksi fluoresoivilla polystyreeni partikkeleilla. Partikkelit saatiin onnistuneesti virtaamaan kanavien läpi, mutta niiden dielektroforeettinen ohjaaminen epäonnistui. Tähän syynä oli luultavasti viallinen elektrodi. Uuden sirun valmistus ei ollut mahdollista laitoksen ollessa suljettuna covid-19 pandemian vuoksi. Sirun valmistusohjeet ja niiden parantamisehdotukset antavat kuitenkin vahvan perustan projektin jatkamiselle.

Avainsanat: Mikrofluidiikka, lasin märkäetsaus, dielektroforeesi, solujen lajittelu, valmistus

Acknowledgements

First, I would like to thank the University of Jyväskylä for granting the facilities of the Nanoscience centre where I could conduct my experiments and work with my passion. It gave me the possibility to work with a subject regarding my favourite disciplines, Biology and Physics. My biggest thanks go to my supervisor Andreas Johansson who granted me such an interesting subject, shared his great expertise, and was always ready to help and guide me through all the challenges.

A lot of credit goes for many others as well. Süha Uğur Öçal helped me jumpstart my research and thought me many skills I needed for this project. Guidance and shared expertise were also granted to me by Gianmario Scotti, Jyrki Manninen, Veli-Mikko Puupponen and Marja Tiirola. I would like to express my gratitude for the colleagues and friends who made my time in the cleanroom enjoyable. Working with all these wonderful people, I could truly see that the cornerstone of conducting scientific research is collaboration.

I also owe a special thanks for my family and my lovely girlfriend Nina Nakari, who supported me and made my thesis writing during a pandemic feel like a wonderful time. Lastly, I would like to thank my friend, Oskar Celik, who studied with me through the hard times and the good: Shâttâl hâttâk patron adam.

Peter Balogh

Contents

1 Introduction

Microfluidics is a field where systems operate with smaller quantities of fluids than that of a nanolitre (0,001 mm^3). Working with such small volumes allows high speed and precise localisation for analysing small particles. Today, microfluidics is mainly used for molecular analysis, but it started off in the 1950's being a part of ink jet printer manufacturing [1]. From there on microfluidics developed after the cold war to field-deployable systems for detection of biological and chemical hazards. In 1980 the rapid growth of molecular biology genomics pushed the development for high throughput DNA sequencing. Finally, the development of the silicon microelectronics contributed with their influence. Photolithography methods could be used for fabricating microfluidics which allowed further complexity being added on chips, such as electronical detection mechanisms. [2]

Microfluidics give the possibility for cell separation and analysis. Resulting from the small volumes, laminar and high flow speed is achievable. Thus, single cells can be guided through channels and analysis with a high throughput achieved. One important application for this is the separation of individual cancer cells from blood. For cancer treatment, thorough analysis of the cells is required to find out which drugs can work on the specific cancer of an individual. The cells could be screened from blood thus requiring no physical operation, which is important for tumours in difficult areas (e.g. the brain). Fast sorting is required because of their low concentration in blood, circulating cancer cells can be as rare as one in 10^8 blood cells [3]. This sets the requirement fast analysis; the throughput should be over the kHz range to be practical.

There are multiple ways for sorting and detecting cells. Optical, thermal, chemical, acoustic, mechanical, magnetic and electrical techniques have been used for cell sorting [4, 5, 6]. To differentiate between cells their intrinsic properties, such as size, refractivity or electrical properties can be exploited. One method is to label a cell with a biological marker. For example, an antibody attached to a fluorophore can label specific proteins or cells selectively. The availability of various biological labels allows cells to be differentiated by fluorescence, radioactivity or by a change in their electromagnetic properties [7]. Dielectrophoresis is a phenomenon where a

force can be exerted on a polarisable particle using a non-uniform electric field. It allows control of unlabelled cells and is one of the fastest sorting methods [6].

A highly popular method for microfluidic device fabrication is “soft lithography”. It includes the use of polymers such as Polydimethylsiloxane (PDMS) to create a mold of microstructures. Although it is an inexpensive and fast method capable of creating complex structures like valves and pumps, it has its limitations [8, 9, 10, 11]. PDMS can swell because of organic solvents and thereby damage the structures. [12]. Polymers also have limited chemical, mechanical and thermal resistance. In addition, they restrict low wavelength light (400 nm) required for laser induced fluorescence spectroscopy [10, 13]. Amongst the huge spectrum of microfluidic devices, rarely a pure glass device is manufactured because soft lithography methods being much easier and cheaper. Glass based microfluidics have three main advantages in biological analysis, they are chemically, thermally and mechanically stable and are transparent in the visible light wavelength region. The mechanical stability allows to create high pressure, thus high throughput systems. The chemicals stability together with thermal stability allows various solvent usage and cleaning possibility of clogged devices for repeatable use [14]. The isolating and heat dissipation properties of glass also allow for high-voltage and frequency dielectrophoretic sorting [15]. Sorting cells with a 100% accuracy [16, 17] or high throughput methods [6] have been developed in the past. Sciambi and Abate have even manufactured a device capable of 30 kHz sorting with over 99% accuracy [18]. Regardless, high speed together with 100% accuracy has not yet been shown.

Dielectrophoretic droplet sorting in a glass device has been demonstrated by Ján Borovský for sorting carbon nanotubes at a femtolitre scale [19]. The aim of this thesis is to upscale such a device to be capable of single cell, high throughput, dielectrophoretic sorting. It would be the a part of a microfluidic chip complex, where cells are pre-sorted to higher concentrations using inertial sorting (capable of sorting 3×10^8 cells/s [20]) and then individual sorting done with dielectrophoresis. Here, the fabrication process is developed to realise a microfluidic chip suitable for dielectrophoretic sorting using fluorescence spectroscopy. The process is conducted using basic microfabrication methods; e-beam lithography, thin film evaporation, and wet etching.

2 Theoretical background

2.1 Microfluidic flow

Dealing with fluids in the dimensions of micro- to femtolitres characterises microfluidics. The channel diameter that is used to transport the fluid ranges in the micrometre range. These small dimensions grant a benefit over larger volumes. The forces and phenomena dominating at the microfluidic scale differs from its scaled-up counterpart; These are surface tension, diffusion, fluidic resistance and energy dissipation. Out of the many dimensionless numbers that describe the microfluidic environment the most important regarding this thesis will be presented.

Reynolds number R_e describes the ratio of inertial forces to viscous forces in fluids. It is defined as

$$R_e = \frac{\rho u d}{\mu} \tag{1}$$

where u is the flow speed, d is the diameter of the channel, ρ the density and μ the viscosity of the fluid. The number shows whether the flow described is turbulent or laminar; R_e smaller than 2000 suggesting a laminar flow. Because of the linear dependence of channel diameter microfluidic channels grant typically a low Reynolds number (R_e <1). Laminar flow grants the benefit of precise flow control of the fluid and the particles within. It is possible to flow two different steams of fluid in the same channel without them mixing, allowing the particles to diffuse from one flow to another. [10]

The flow in microfluidic channels can be described by the Poiseuille equation. It describes the pressure drop in a pressure driven flow. It assumes an incompressible Newtonian fluid, which is applicable to microfluidic systems [19]. For a cylindrical pipe, the flow speed is parabolic, slowing down near the edges and increasing towards the centre. The volumetric flow rate Q of a Poiseuille flow can be expressed as

$$Q = -\frac{\pi r^4}{8\mu}\frac{dP}{dz} \tag{2}$$

where r is the radius of the pipe, μ the fluid viscosity and P is the pressure along the pipe axis z [10]. Although the profile of the manufactured channels in this thesis is

different from a circular pipe, this gives an understanding of the features governing the velocity of a laminar flow. For precise flow control the channel dimensions and the inlet/outlet pressures play an important role. Given an incompressible fluid, the microfluidic channels can be modelled by the laws of electric currents. The hydrodynamic resistance R_{hyd} of a constant flow rate can be expressed as

$$\Delta P = R_{hyd} Q \tag{3}$$

where ΔP is the constant pressure drop. This can be related to Ohm's law $U = RI$ and the same type of circuit analysis can be performed to microfluidic channels. At junctions and intersections in Kirchhoff's laws can be applied, meaning the sum of flow rates entering and leaving any node in the circuit is zero. This means that if the flow is to be divided evenly at a Y-junction, the hydrodynamic resistance of both outgoing channels needs to be the same. [21] Combining equations 2 and 3 we can see that $R_{hyd} \propto \mu / r^4$, meaning that the resistance scales unfavourably for a pressure driven flow microfluidic flow. Driving viscous fluids through small channels will require high pressures and correspondingly durable devices.

2.2 Fluorescent detection

The absorption of electromagnetic radiation into an atom or excites it to a higher energy level. An excited electron returning to its lower energy state will emit its excess energy as a photon. The emitted light is called fluorescence. The electron loses a small amount of energy to vibrational relaxation during the short lifetime of the excited state before emitting a photon and returning to its ground state. This is called the Stokes shift and causes the emitted photon to have a longer wavelength than the exiting one (Figure 1a). This phenomenon is often used in biology to detect and label cells, cell organelles and even single molecules. Fluorescent molecules (fluorophores) are commercially available with a wide variety of excitation/emission wavelengths, molecular structure, and quantum yield (photons emitted per absorbed). The main advantage of fluorescence is the shift in emission wavelength. A shorter wavelength monochromatic light can be used illuminate the sample whilst only the emitted light is detected by filtering the shorter wavelengths out (Figure 1c). Fluorescent labels can have almost 100 % accurate binding specificity and can have increased fluorescence up to an order of magnitude when in the correct binding site

or environment, for example, within the cell. These labels are organic and deliverable within a cell granting the possibility for live cell labelling and imaging. [22]

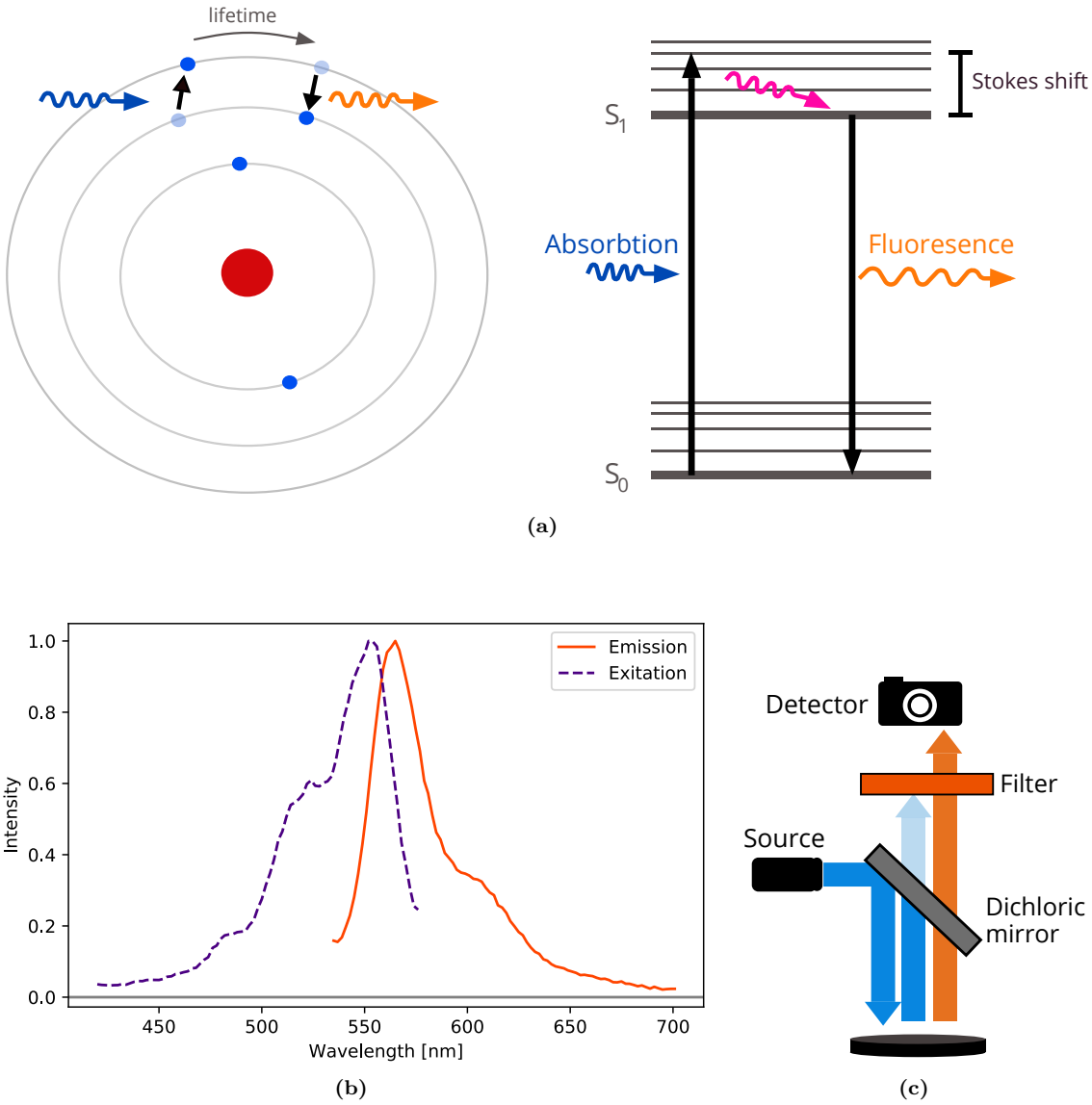

Figure 1. a) Basic principle of fluorescence. b) The excitation/emission wavelength of a fluorescent dye (Alexa Fluor 555) as an example. c) The simplified idea of fluorescence imaging.

A characteristic binding site is required to achieve targeted protein labelling, but cancer cells include mostly the same proteins as a healthy cell. To distinguish them from normal cells the Warburg phenomenon can be exploited. It is a fundamental characteristic of cancer cells in which fermentation is preferred over phosphorylation as an energy acquiring mechanism [23]. As a result, the glucose intake of cancer cells is significantly higher compared to regular cells. Using labelled glucose molecules

that are altered to prevent their metabolization, the labelled glucose will accumulate in high-glucose-using cells. This is a common method used in positron emission tomography (PET) scans with radioactive labels to detect tumours. There are also glucose labels like 2-NBDG (2-[N-(7-nitrobenz-2-oxa-1, 3-diazol-4-yl)amino]-2-deoxy-D-Glucose) which can be used for fluorescent detection of cancer cells [24]. Because of the short lifetime (nano seconds) of the excited state in fluorophores, fluorescence is a suitable method for fast throughput imaging.

2.3 Dielectrophoresis

2.3.1 Theory

Dielectrophoresis (DEP) is a phenomenon, where a non-uniform electric field can cause a force on a polarizable particle. This phenomenon can be used to move and separate label-free particles. A uniform electric field would cause a uniform charge-distribution on an polarizable particle therefore creating a net-force equal to zero. Respectively, a non-uniform electric field will cause the positive and negative charge accumulation inside the particle to be uneven, causing a net force (Figure 2b). The direction and the magnitude of the force will depend on the particle's and mediums polarizability and the electric field [25]. The term dielectrophoresis was already introduced in 1951 by Herbert A. Pohl [26]. DEP has since gained popularity in microsystems because of its simplicity and favourable scalability $F_{dep} \propto V^2/L^3$, where V is the applied voltage and L the distance from particle to electrodes. This means that on a smaller system, less voltage is required to achieve the same force F_{dep} [27].

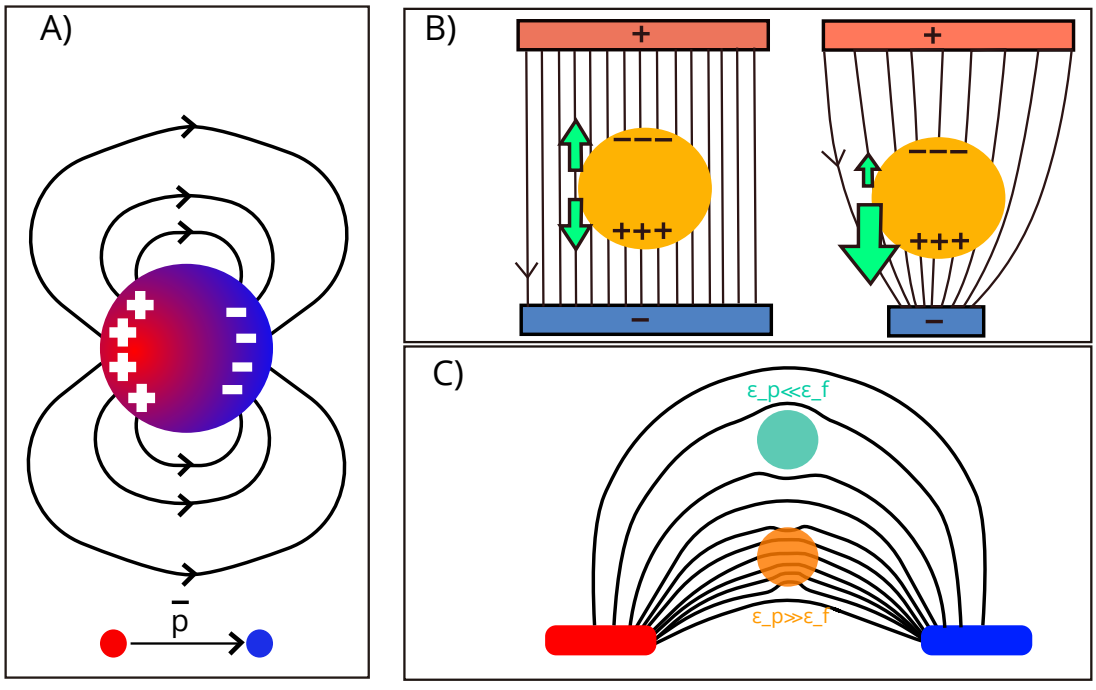

Figure 2. Visualisation of DEP. A) A Polarised sphere has a dipole moment ($\vec{p}$). B) The net force in a uniform and non-uniform electric field C) Particle and medium permittivity effect on electric field

There are multiple mathematical models describing DEP [28]. They vary on their complexity and demand on computational power. Here we will be presenting a simplified and general method for the DEP force calculations which has been presented by a number of review articles [4, 29, 30, 31]. The force experienced by a dielectric particle can be expressed as

$$\vec{F}_{\mathrm{DEP}} = \vec{p}\vec{\nabla}\vec{E} \ , \tag{4}$$

where $\vec{p}$ is the dipole moment vector, and $\vec{\nabla}\vec{E}$ the gradient of the electric field. The dipole moment depends on the shape of the particle, for a perfect dielectric uniform sphere, it can be expressed as

$$\vec{p} = 2\pi\epsilon_f R^3 \mathrm{Re}[f_{CM}]\vec{E} \ , \tag{5}$$

Here R is the radius of the particle, ϵ_f the absolute permittivity of surrounding fluid and $\mathrm{Re}[f_{CM}]$ the real part of the Clausius-Mossotti factor (CM) [29]. The CM factor for a spherical particle is

$$f_{CM} = \left(\frac{\epsilon_p^* - \epsilon_f^*}{\epsilon_p^* + 2\epsilon_f^*} \right) \ , \tag{6}$$

Where ϵ^* the complex absolute permittivity of the particle (p) and the surrounding fluid (f). They are related to conductivity σ and the angular frequency $\omega = 2\pi f$ of the electric field as

$$\epsilon^* = \epsilon - \frac{i\sigma}{\omega} \ , \tag{7}$$

i being $\sqrt{-1}$. Combining equations (4) and (5) we get and expression for the force

$$\vec{F}_{\mathrm{DEP}} = 2\pi\epsilon_f R^3 \mathrm{Re}[f_{CM}]\vec{\nabla}(\vec{E}\cdot\vec{E}) \tag{8}$$

For an AC potential the time average of the force can be expressed as

$$\langle \vec{F}_{\mathrm{DEP}} \rangle = 2\pi\epsilon_f R^3 \mathrm{Re}[f_{CM}]\vec{\nabla}(E_{RMS}^2), \tag{9}$$

where E_{RMS} is the root mean square value of the electric field $E = \mathrm{Re}[E_0 e^{i\omega t}]$. When the CM factor (Eq. 6) is expanded (Eq.7) we can see the frequency dependence.

$$f_{CM} = \left(\frac{(\epsilon_p - \epsilon_f) + \frac{i}{\omega}(\sigma_f - \sigma_p)}{(\epsilon_p + 2\epsilon_f) - \frac{i}{\omega}(\sigma_p - 2\sigma_f)} \right) \tag{10}$$

Examining the electric field at low ($\omega = 0$) or a high frequencies ($\omega = \infty$) we can see that the CM is reduced to

$$f_{CM} = \frac{\sigma_p - \sigma_f}{\sigma_p + 2\sigma_f}, \text{ when } \omega \to 0 \tag{11}$$

$$f_{CM} = \frac{\epsilon_p - \epsilon_f}{\epsilon_p + 2\epsilon}, \text{ when } \omega \to \infty \tag{12}$$

At high frequency, the particle acts like a capacitor and is dominated by its permittivity. Whereas, at very low frequencies the current in the particle moves in phase with the electric field thus the conduction is the dominating factor [8, 29, 32]. From the CM factor (Eq.6) we can also see that the permittivity of the particle and the surrounding medium determines whether force is pushing or pulling towards the region of stronger electric field. If the particle is more polarizable ($\epsilon_p > \epsilon_f$) a positive force (pDEP) is pushing towards he higher field and vice versa (Figure 2c). We can also see from $\epsilon_p >> \epsilon_f$ and $\epsilon_p << \epsilon_f$ that the pDEP can be twice the magnitude of the negative DEP force (nDEP). The most important points arising from these equations are:

I The Force is zero in a uniform field ($\nabla E = 0$).

II The force depends non-linearly on the field magnitude (E^2) and showing that both an AC and CD field can cause a DEP force.

III The dependence on particle volume $\propto R^3$ allows separation of particles based on size.

IV Due to conductivity and permittivity dependence of the medium and particle, the DEP force can be pulling or pushing. By changing the frequency, there is a crossover-frequency where pDEP changing to nDEP can be achieved. [33]

The simplifications made when deriving Eq.9 need to be taken into consideration, meaning that the particle needs to be a perfect homogeneous dielectric sphere with no net charge. In addition, the polarisation of the particle is assumed as a simple dipole moment, even though a non-uniform field is causing the polarisation. The medium around the particle is considered infinite and not affected by the particle itself. [8] In this thesis the aim is to use DEP for cell sorting. They have various shapes and are not uniform. Cells contain membranes, cytoplasm and organelles. In order to have higher accuracy for simulations more precise mathematical models can be introduced

at the cost of computational time [8, 28, 30, 32]. But, even with its simplifications, this model is sufficient to describe the DEP system and the underlying physics.

2.3.2 Single shell model

The CM factor for a mammalian cell has characteristic properties. As an example, a white blood cell has been demonstrated [4]. At low frequencies ($< 100\,\mathrm{kHz}$) the cell is less polarizable than a typical ionic solution thus causing a nDEP effect. Similarly when going to MHz frequencies, the conductivities of the solution and the cell will matter more, thus resulting in a pDEP in low conductivity solutions ($5{,}5 \times 10^{-6}\ \frac{\mathrm{S}}{\mathrm{m}}$ for DI water [34]). At GHz range, the permittivities will be mainly compared (Eq.12) and likely to cytoplasmic proteins, the permittivity of the cell is low compared to water and results in a negative DEP. Although the frequency depends highly on the cell and medium properties, the "single-shell" model (Figure 3) predicts these two cross over frequencies [4, 8, 30, 32]. The single-shell model uses a CM factor where a shell (cf. cell membrane) is accounted for with its own properties. In the single shell model the complex permittivity is

$$\epsilon^* = \epsilon_{mem} \left[\frac{\left(\frac{r}{r-d}\right)^3 + 2\left(\frac{\epsilon^*_{CP}-\epsilon^*_{mem}}{\epsilon^*_{CP}+2\epsilon^*_{mem}}\right)}{\left(\frac{r}{r-d}\right)^3 - \left(\frac{\epsilon^*_{CP}-\epsilon^*_{mem}}{\epsilon^*_{CP}+2\epsilon^*_{mem}}\right)} \right] , \tag{13}$$

where r is the cell radius, d the thickness of the membrane, ϵ^*_{CP} and ϵ^*_{mem} are the complex permittivities of the cytoplasm an the membrane. A simulation of the CM factor using the single shell model for HT-29 cells is shown in Figure 3. The result is from a Java simulator published by Cottlet et al [30].

For comparison, a simulation was also done with the same cell having a larger radius and one being submerged in DI-water ($\sigma_{DI} \approx 0$). In reality, the change in medium conductivity can affect the membrane conductivity up to 2 orders of magnitude, which has not been accounted for in this simulation [35]. This simulation gives a sense for order of magnitude of the frequency to be used in our experiment. It also shows that cells with different properties, such as size, electrical properties and shape, can be separated with DEP with a correct frequency. Around the crossover frequency cells can experience nDEP or pDEP depending on their properties. Separating cancer cells from blood using DEP has already been demonstrated by multiple publications [3, 36, 37, 38].

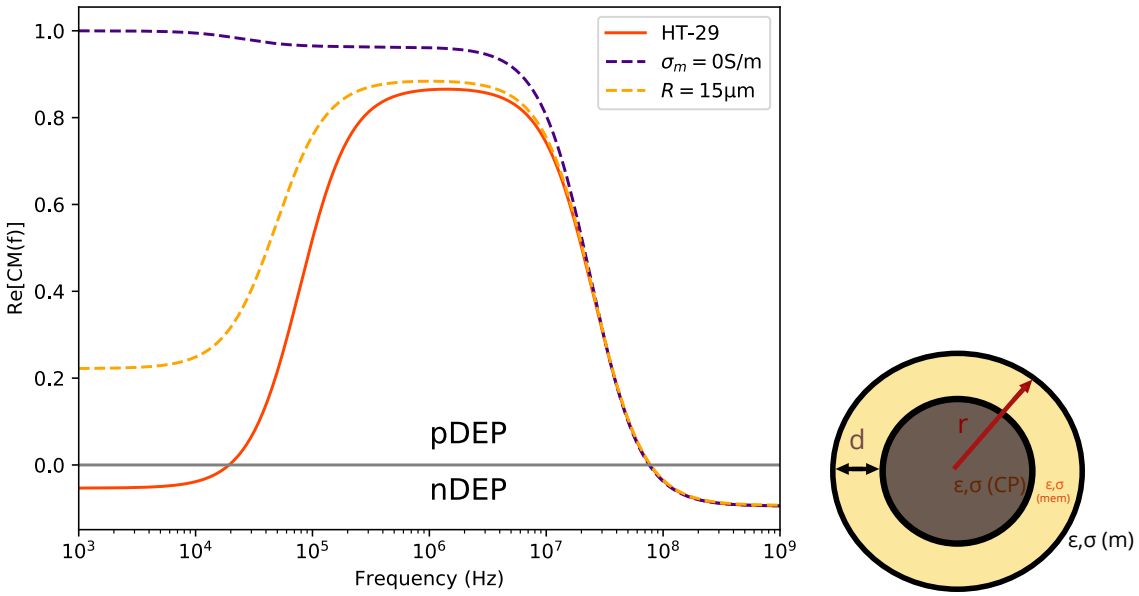

Figure 3. (Left) CM factor for Human colon cancer cells (HT-29) has been simulated with MyDEP tool [30]. The values used in the simulation are presented in Table 1. A change in cell radius and a change in media was also simulated for comparison. (Right) The single shell model.

Table 1. The literacy values of the simulated HT-29 cell's permittivity (σ), conductivity (ϵ) and radius (r) [35]. The subscripts refer to the cytoplasm (CP), cell membrane (mem) and the surrounding medium (m).

σ_m (S/m)	ϵ_{mem}	ϵ_{CP}	σ_{mem} (S/m)	σ_{CP} (S/m)	r (µm)
0.01	4.68	68.31	$6.63e-6$	0.279	6.6

2.3.3 Choosing DEP

For successful high throughput cell sorting, the correct parameters are needed to be chosen for our DEP system by accounting for all the challenges and advantages. The electrodes for DEP can be fabricated to be in contact with the sample fluid or contactless, and DEP can be achieved with using AC or DC currents. The field strength can be chosen by varying the potential or the dimensions of the electrodes. For nDEP or pDEP the correct frequency needs to be chosen for the AC alternative. As an outcome, the DEP force needs to out scale drag-, buoyancy-, and electrothermal forces together with Brownian motion (not a problem for >1um particles) [32].

For DEP applications, the most common way is placing the electrodes in contact with the liquid. This allows the particles to be closer to the electrodes thus perceiving a higher gradient which allows for better control precision [4]. Unfortunately, contact

with the sample fluid can lead to many problems, especially with biological samples. Electrode polarization, dissolution, bubble formation, contamination of the fluid and fouling can affect the operation. Especially in DC systems electrochemical effects can produce H_2 and O_2 gas. Joule (resistive) heating causes a problem, already at 4°C above body temperature (37°C) it can lead to mammalian cell death. [4, 25, 32]. Using contactless electrodes, bubble formation, contamination and fouling are completely eliminated. The medium is then only in contact with the substrate. This also reduces heating from a high intensity light, e.g. fluorescence inducing light, absorbed by the electrodes. For contactless electrodes AC is the better choice, because DC would require higher voltages for sufficient DEP, which leads to joule heating. A high frequency electric field is also less stressing on a cell membrane, which have voltage sensitive proteins, than that of a DC field [4].

3 Methods

3.1 Cleaning and activation

Cleaning the glass chips before the fabrication steps is of critical importance. Most of the process steps require dust/particle contaminant free surfaces. The two main reasons are for good thin film adhesion and thermal bonding. Surface contaminants cause bad adhesion and pinholes in thin films. In thermal bonding of the chip and the cover-glass, they cause Newton-rings; around the contaminant a colourful ring shape can be perceived resulting from the opening between the two glass surfaces. This opening can lead to leakage and destruction of the chip.

Cleaning the glass was done by scrubbing the surface with cotton tips in acetone, then sonicating and rinsing in Isopropyl Alcohol (IPA). Acetone is a good organic solvent for general cleaning, removing fingerprints and dissolving glue from tape residue. The mechanical scrubbing together with sonification loosens and removes solid contaminants. The final rinse with IPA removes the traces of acetone and evaporates quickly leaving a spotless surface. To ensure cleanliness, the glass can be dried with N_2 blowing and checked against light for contamination. To minimize particle contamination the chips should be transported in deionised water. Despite being in a cleanroom, ambient air is a potential risk for contamination. For the removal of metal and organic contamination and glass surface activation, Piranha solution was used [39]. Piranha is a strong oxidizing agent consisting of sulfuric acid (H_2SO_4) and hydrogen peroxide (H_2O_2). The ratio can be tuned, but if the concentration of H_2O_2 is over 50% an explosion can occur [40]. The solution is heated to 100 °C to increase the reaction speed but only after it has cooled after mixing because the reaction is highly exothermic. The solution also hydroxylates the glass surface (activation) adding -OH groups [41]. The hydroxylation helps thin-film adhesion and is necessary for the bonding of glass. Surface activation can also be achieved with RIE (Reactive Ion Etching)[42]. High frequency O_2 plasma treatment can also remove contamination and hydroxylate the glass surface. It is a faster method compared to Piranha clean but is not as effective than the highly reactive aforementioned chemical clean.

3.2 Thin film deposition

3.2.1 Evaporation

The etch mask quality is crucial for etching, thus it is important to understand the deposition mechanism to fix film quality problems. Thin film deposition on a substrate is one of the key methods in microfabrication dating back to the 19th century [43]. Today, the production of thin films has been mastered mainly for the needs of the semiconductor industry. Thin films can become a permanent part of the substrate (e.g. electrodes, semiconductors, capacitors, insulators or protective elements) or act as etch masks [39]. One of the many methods of producing thin films on a substrate is evaporation, where the material is evaporated from liquid form or sublimated. When the evaporated material hits a cooler surface it will deposit, forming an amorphous film. Evaporation requires the vapour pressure to be higher than of its surroundings. Naturally, there are two ways to achieve this; Either the material's vapour pressure is increased by heating or the vapor pressure of the surrounding gas is reduced by lowering the pressure. The evaporation rate ϕ (flux of the material) can be expressed using the vapour pressure P_V as

$$\phi = \frac{P_v(T)}{2\pi m k_b T} \tag{14}$$

where k_b is the Boltzmann constant, m the mass, and T the temperature of the material [39].

3.2.2 E-beam evaporation

The method used in this thesis was Electron-beam physical vapor deposition (EBPVD) or E-beam evaporation for short. In EBPVD the kinetic energy of electrons is used to heat the target material. An electron source is created by joule heating a tungsten (3660 K melting point) filament to cause thermionic emission [39]. The released electrons are then accelerated by an applied voltage and guided into a crucible using a magnetic field (Figure 4a). The Kinetic energy of the electrons heat the target material leading to its evaporation. When the correct evaporation rate is achieved, a shutter covering the substrate is removed allowing the evaporated material to deposit on the substrate.

The biggest concern in thin film deposition is contamination. Impurities can

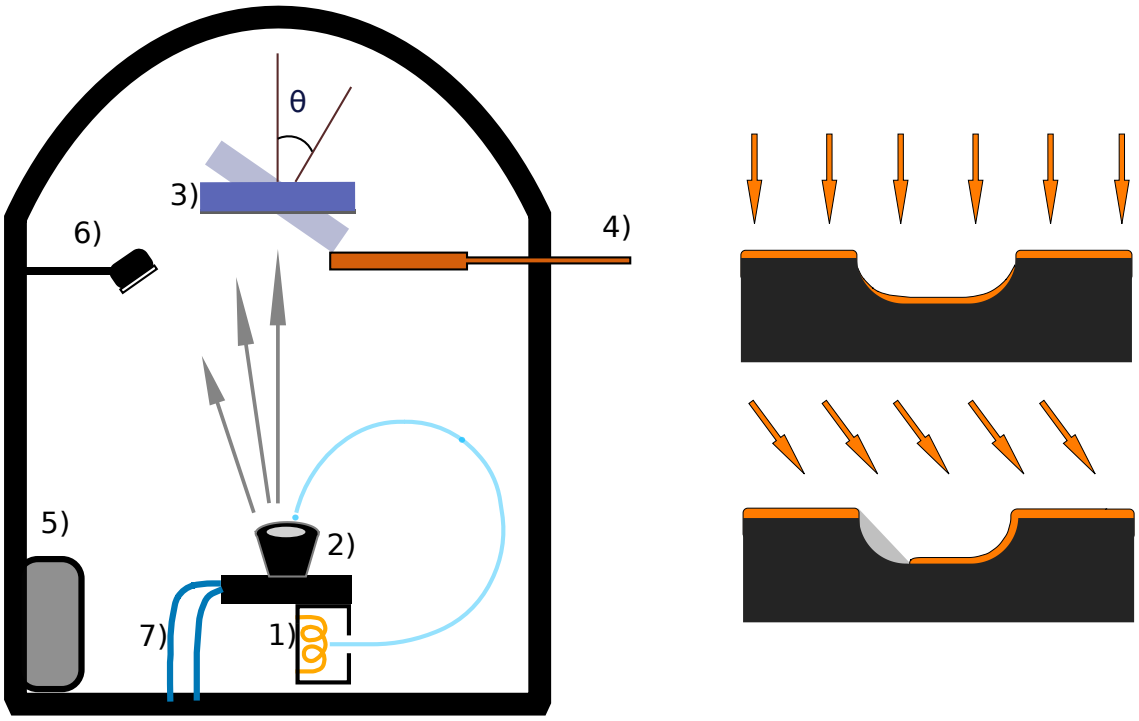

(a) Evaporator

(b) Line of sight coverage

Figure 4. a) Schematic of an e-beam evaporator. 1) Electron source 2) Crucible containing the target material 3) Substrate with variable angle 4) Shutter 5) Pump 6) Thickness detector 7) Water cooling. b) Comparison of direct and angle evaporation.

cause bad film adhesion, pinholes and change in chemical composition of the film rendering it useless for its applications. The main sources for contamination arise from impurities in the evaporation material, the crucible, cleanliness of the chamber, or the gases present in the evaporation chamber. Evaporation materials are usually sold with high purity (over 99,99 %), but they easily contaminate if stored improperly. For example chromium oxidises quickly when in ambient air.

To avoid the evaporated material colliding with gas molecules, their mean free path should be longer than the distance from the crucible to the substrate. The mean free path λ can be derived from the kinetic theory of gases to be

$$\lambda = \frac{k_b T}{\sqrt{2}\pi d^2 P} \tag{15}$$

T being the temperature, P the pressure and d the effective cross-section of the particle. In an ideal case, the evaporated material travels directly to the substrate. The main advantage of using EBPVD is that the beam heats only the target material and not the crucible. Keeping the crucible at lower temperature prevents

the evaporation of the crucible itself or unwanted chemical reactions between the crucible and the material. [39]

Collisionless transport results in a line of sight coverage which can lead to non-uniform film thickness. The thickness uniformity depends on the position of the substrate to the source. The substrate edges with a different angle or distance from the source will result in a different film thickness compared to the centre of the substrate. Small thickness variations are not important parameters for an etch mask, but the coverage is crucial. It can be influenced by the evaporator design. A longer distance between source and substrate, rotation and angle variation of the substrate can all affect the coverage (Figure 4b). To produce pure films, a low pressure is required with a high deposition rate [43]. The deposition rate can be tailored by increasing the acceleration voltage of the electrons and hence the temperature of the target material. The rate can be measured inside the chamber with almost atomic layer precision by using a quartz crystal. The deposited mass on the crystal changes its resonant frequency, which can be precisely measured [39].

Before evaporation, adhesion and stress of the film should be considered. Unless special combinations of substrate and evaporation materials are picked, the adhesion will be poor. If the film material isn't compatible with the target surface, adhesion layers can be used. Noble metals like gold aren't reactive and will not form metal-oxide bonds, which are a necessity for good oxide surfaces adhesion. For example the adhesion between gold and glass is very poor. A strong adhesion can be achieved with the use of TiW, Ti or Cr adhesion layers, with a few nanometres of an adhesion layer being sufficient [44]. Substrate cleanliness is the next important factor for film adhesion because impurities will not allow bond formation. Internal stress of the film will weaken the adhesion. Although evaporated films do not suffer from stresses arising from a crystal structure, they experience tensile stress during cooldown after deposition due to having higher temperature during deposition and typically higher thermal expansion coefficient than the substrate (Figure 5). Therefore, some evaporators have the possibility to heat the substrate. [39]

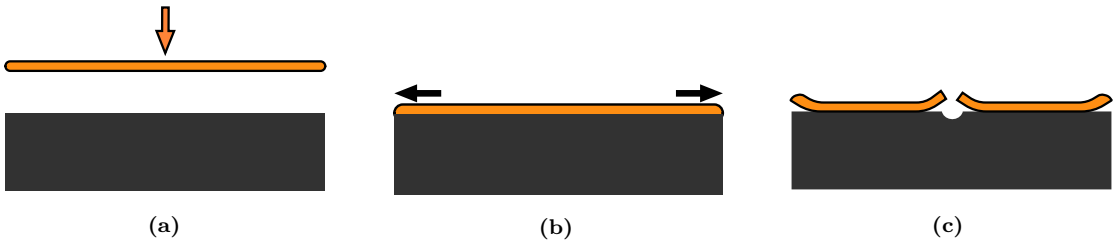

Figure 5. Tensile stress in evaporated thin-films. a) When evaporated, the target material is hot. b) Cooling on the substrate will cause the film to shrink, resulting in stress. c) If a hole is made in the film (by pinhole or etching) the stress will bend the film from the surface.

3.3 Lithography

The idea of lithography is print a pattern on a surface by changing the surface properties. Photolithography is indeed the main method used in microfabrication. The idea is to use a photosensitive material (resist) and expose it to light through a mask, that allows light to penetrate only at desired areas. The exposed areas undergo a chemical reaction which is used to generate a pattern. The exposed areas (positive resist) or the unexposed areas (negative resist) can be then chemically removed (Figure 6). Photolithography serves well the microfabrication industry, because hundreds of copies can be printed using a single mask. Photolithography is the most popular method in microfabrication. The drive to imprint smaller features (Moore's Law) has led to the development new methods. [39, 45]

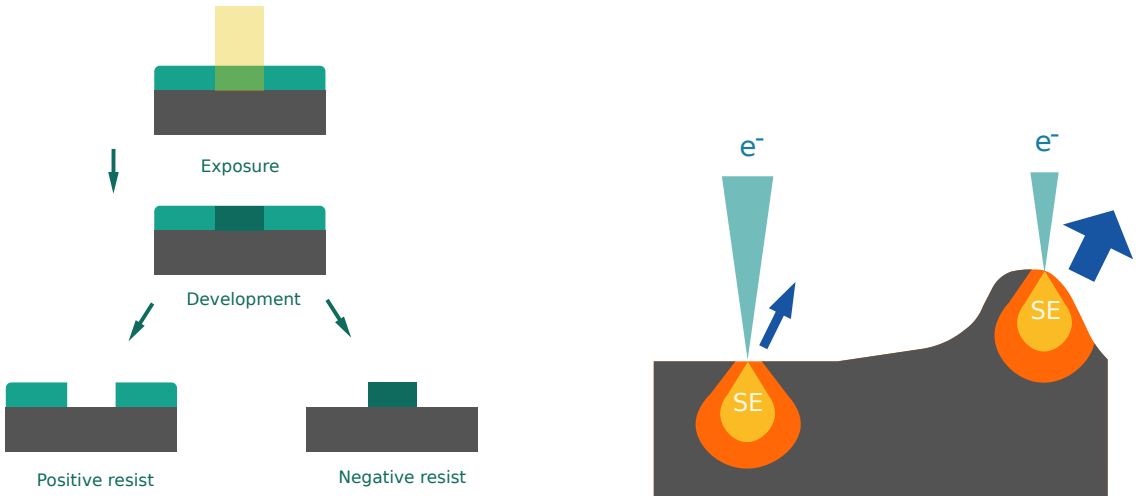

Figure 6. (Left) Positive and negative resist exposure and development (Right) SE generation. SE's can can escape from close to surface, an inclined surface will produce more SE's thus increasing the contrast.

3.3.1 Electron microscope

Electron microscopes were developed to overcome the resolution of optical microscopes, which were limited by visible lights diffraction. The first Scanning Electron Microscope (SEM) was built by Max Knoll in 1935 [46]. SEM follows the basic principles of an electron microscope. This means that it contains an electron source, usually a tungsten filament which emits electrons via thermionic emission when a sufficiently high voltage is applied. Much like in optical microscopes the beam is then focused, but by the magnetic field of coils. SEM is not limited by the diffraction limit because of the small wavelength of electrons. Combining the de Broglie wavelength $\lambda = h/mv$ with kinetic energy $E_{kin} = 1/2mv^2$, we can get an expression for their wavelength as

$$\lambda = \frac{h}{\sqrt{2mE_{kin}}} \tag{16}$$

where h is Planck's constant and m the mass of an electron. The electrons can be accelerated by an applied electric field to acquire the desired energy (typically 10-100 keV) [47]. An electron with a kinetic energy of 20 keV would have a wavelength of 8,7 fm. The electron beam is focused to an area of 0,4-5 nm (pixel size) and the sample is raster scanned. Each pixel is then analysed separately, and the data recorded.

SEM uses mainly the detection of secondary electrons (SE) which have lower kinetic energies than the backscattered ones. The SE emission is caused near the sample surface due to inelastic scattering, produced by ionisation. SE's can escape the sample only from near the surface thus revealing information about the sample topology (Figure 6). At a sharp profile, SE emission is increased leading to increased electrons in the detector, resulting in a brighter pixel. E-beam lithography has the same principle as photolithography, but instead of photons, the resist is exposed through electron bombardment which can be achieved with an electron microscope. When using an SEM, the sample needs to be able to withstand the vacuum inside the microscope. It also needs to be somewhat conducting to avoid accumulation of electrostatic charge.

3.3.2 Resists, PMMA

Resists consist of carbon-based polymer chains that react to electromagnetic wave exposure. As in photoresists the chemical reaction in e-beam resists is either the cross-linking or fragmentation of chains. In a positive resist the polymer chains are disrupted making them shorter, which can dissolve easier in an organic solvent (developer) (Figure 7). Likewise, in negative resist longer chains are formed, thus making the exposed areal less soluble. One of the first developed and the most popular e-beam resist is Polymethyl methacrylate (PMMA). It has the capability of acting as both positive and negative resist. PMMA is highly sensitive (requires little exposure compared to other e-beam resists) and has a resolution of 10 nm but it has poor etch resistance. For the development of PMMA, MIBK:IPA (Methyl isobutyl ketone: Isopropyl alcohol) is used and for removal, Acetone. [47]

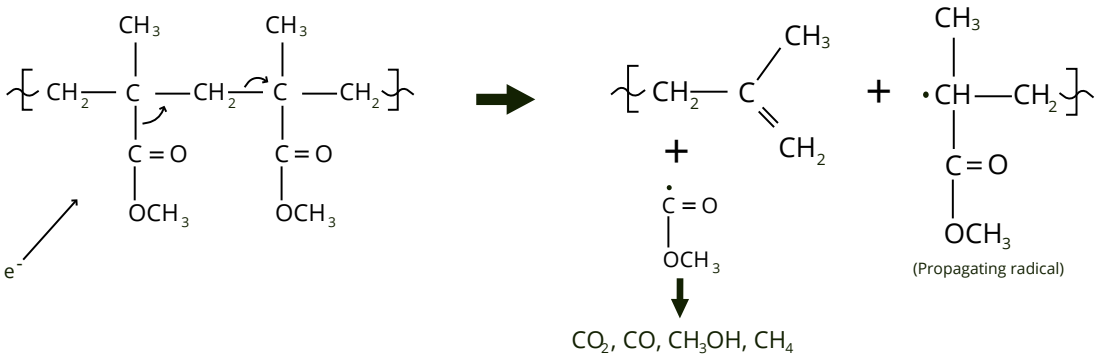

Figure 7. The mechanism of PMMA polymer scission due to e-beam exposure. Adapted with permission from [48]. Copyright 1991 American Chemical Society.

Selection of the correct resist is important for achieving the desired result. Multiple resists are available with different sensitivities, contrast and developers. The composition of the resist itself can also be varied. For example, both PMMA 950K A4 and -A11 were used in this thesis. 950K refers to the molecular weight and "A" to the solvent (4 % PMMA in Anisole). To achieve a good lithographic process these parameters should be optimized:

I Exposure dose

II Development time

III Resist adhesion to substrate

IV Resist thickness

In the case of a glass substrate solely PMMA cannot be used. It is not conductive and will cause charge accumulation, which will have a repelling effect on the incoming electrons. Charge accumulation will lead to unwanted exposure areas, ruining the sample. Usually a thin metal film or a layer of conductive resist is used to ground the sample.

3.4 Wet etching

Etching is the subtractive process in microfabrication. Material is etched in order to create cavities, patterns or just to remove unwanted material. Etching can be divided into physical or chemical methods. Physical methods consist of eroding the material, for example, with a focused ion beam. Chemical etching is based on chemical reactions removing the material.

In wet etching the substrate is simply dipped into a chemical solution which will react with the target material. In most cases a mask is used to allow the chemical reaction to happen only at the desired areas. When choosing an etchant, selectivity is the key factor. The aim is to have the etchant reacting specifically with the target material leaving the mask and other materials unspoilt. A faulty or deteriorated mask will lead to the destruction of the sample. Wet etching is a highly tuneable process. Chemical information and reactions of different etchants are widely available thanks to the microfabrication industry [49]. After finding the correct etchant, the etch rate can be tuned by etchant concentration, temperature and stirring. Compared to physical etching wet chemical etching is faster. The drawback of wet etching is isotropicity. Because the etchant etches typically in all directions, the target material will be etched from the mask opening as much in depth as in the lateral dimension, meaning the ratio of depth:width will always be at least 1:2 (Figure 8). In reality the etch rate can vary in the lateral direction due to the reduced availability of fresh etchant in small cavities. [45]

Glass etching

Wet etching of glass is difficult due to its chemical stability and it is mainly etched with hydrofluoric acid (HF). The generalised etch mechanism is: [50]

$$SiO_2 + 6HF \rightarrow 2H_2O + H_2SiF_6 \tag{17}$$

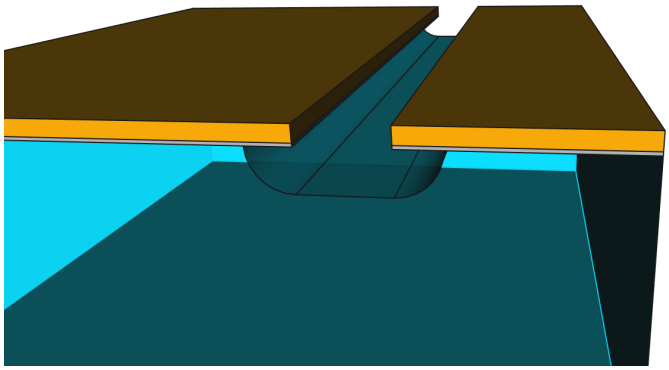

Figure 8. Isotropic etching. The etch rate from the mask opening is the same in all directions.

The challenge with HF is that it is a highly dangerous chemical and for safety reasons, boiling and sonication is not recommended. Additionally, only a few mask materials are chemically inert to it. Using solely a photoresist mask for HF etching has been reported [51, 52], but the most common mask for HF glass etching is the combination of Au and Cr, which are both inert to HF [53, 54]. Other combinations like WTi/Cu and Cr/Cu have also been demonstrated as being able to act as a masking material [55, 56]. From Eq.17 we can see that the reaction depends highly on the concentration of HF. But the formula is applicable only for pure quartz glass. The glass used in this thesis was Soda Lime, which was chosen because of its low cost and high etch rate compared to other glasses [57]. It consists of multiple components which are presented in Table 2. CaO, MgO and Al_2O_3 can form insoluble products

Table 2. The composition of soda-lime glass slides according to manufacturer [58].

SiO_2	MgO	Na_2O	Al_2O_3	K_2O	Fe_2O3	CaO	SO_3
72.20%	4.30%	14.30%	1.20%	1.20%	0.03%	6.40%	0.30%

together with HF, and they can leave precipitations and create “masked” areas for the etchant, which will result in a rough surface. Mixing HCl has proved to dissolve these molecules and result in a better etch surface [53]. The etch rate and surface roughness quality can be further tuned by the addition of HNO_3, H_3PO_4 or H_2SO_4 [59]. In the case of Deep etching (over 10 µm) high etch rates are desirable. There is always a probability for mask defects and the etchant penetrating them. The penetration of the etchant through these defects is constant, so reducing the etch time by having a high etch rate will result in less defects [54]. Other than glass composition, etchant concentration and applied heat, the etch rate can also be

increased by annealing the glass. Annealing reduces stress and redistributes oxides within the glass, leading to a stable etch rate throughout the glass [60].

3.5 RIE

Reactive ion etching (RIE) is a dry chemical and physical etching method where a reactive plasma is used to etch material. In RIE, the substrate is placed within a vacuum chamber, which is then filled with a suitable reactive gas. Capacitively (or inductively) coupled electrodes are connected to a radio frequency (RF) voltage source, generating a plasma in the chamber. The changing electric field ionises the gas molecules and causes the free electrons to accelerate and hit the chamber walls and the substrate. The substrate is kept on an electrode that is capacitively coupled to the source, thus it will accumulate negative charge (negative DC bias), causing the positive ions in the gas to drift towards it (Figure 9). The gas reacts with the substrate material and forms a volatile product which is then pumped from the chamber. This directional particle bombardment is the reason for the anisotropic nature of RIE. The ion bombardment causes physical- and the reactive gas chemical etching. [61]

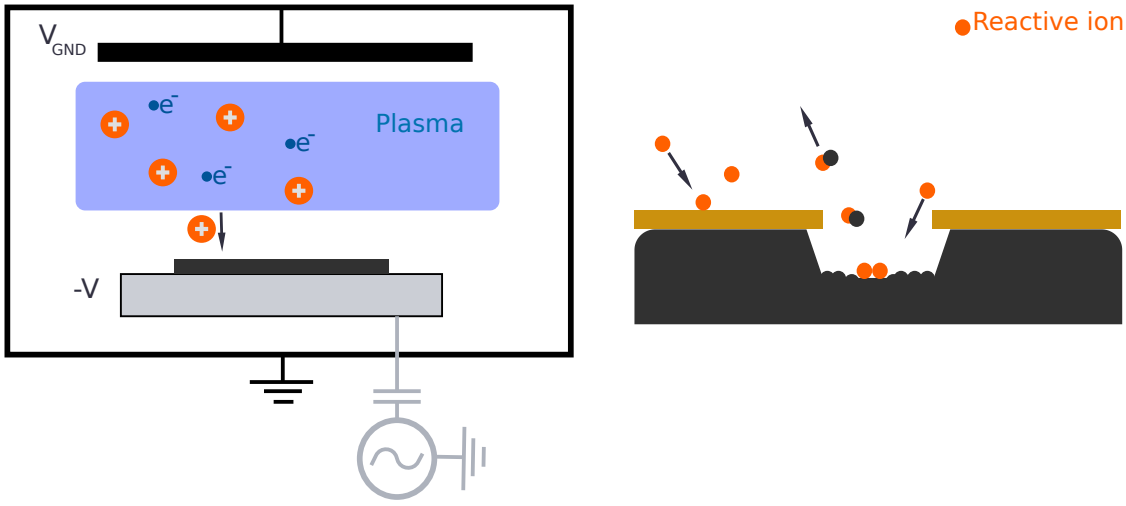

Figure 9. Operation principle of a capacitively coupled RIE system (left) and the anisotropic etching profile (right).

This is only the basic principle of RIE. Multiple parameters such as, RF-power, DC-bias, pressure, gas flow rate and temperature all affect the etching process. All of these need to be tuned, to achieve good anisotropy, correct etch rate, and selectivity. The etch chemistry is defined by the gas chosen. Correct selectivity between mask and substrate, and volatile product formation is critical. There are already many well known recipes for RIE, for example, fluoride based gases (like SF_6) are used for silicon etching. For silicon dioxide, CHF_3 is a common choice because of its selectivity to silicon. It will produce SiF_4 and CO_2 as products which are both volatile (boiling points $-90\,°C$, $-56\,°C$). [39] RIE equipment can be used for cleaning or activating wafers. An oxygen (O_2) treatment can be used to oxidize and remove organic contamination, which can be residues from organic solvents (acetone) or resists. An O_2 plasma treatment will create a silicon oxide surface on the surface of silicon, or in our case, glass. A following rinse in DI water will then grant a hydroxylated surface. Even wafer bonding has been demonstrated with plasma activated surfaces [62, 63]

3.6 Glass bonding

Wafer bonding is often used in microfabrication when two or more wafers need to be merged together. Bonding mechanisms between two materials can be anodic, direct, or adhesive. In our case the cover glass needs to be bonded to the patterned glass to form complete channels. In the case of two glass surfaces, direct bonding can be applied. Activating both to-be-bonded surfaces will cause the surfaces to be saturated with hydroxyl groups. Bringing the surfaces close enough (under 2 nm) van der Waals bonding will occur (Figure 10) [64]. The bond strength depends on surface roughness; the number of bonds depends on the area where distance is short enough between the wafers. This weak bonding can be increased significantly by annealing. High temperatures cause the water molecules to diffuse from the surface into the bulk material, thus allowing covalent bonding between the surfaces;

$$\mathrm{Si-OH + HO-Si} \rightarrow \quad \mathrm{Si-O-Si}$$

The formed bond between the wafers will be as strong as the bulk material itself, hence Thermal Assisted Direct Bonding (TADB). Bonding glass to glass has also the benefit of both surfaces having the same thermal coefficients, thus stress can be avoided. [39]

The bonding procedure consists of substrate cleaning and activation, room temperature bonding, and annealing under slight pressure. The cleaning procedure is extremely delicate because any contaminant will increase the distance between the surfaces and will lead to unsuccessful bonding. The temperature and pressure for TADB needs to be optimised for good bonding strength. The optimised temperature and pressure for Soda-lime glass bonding is determined to be 580 °C, 28 kPa [65]. To achieve the correct pressure, small weights can be used on top of the substrate while in the furnace.

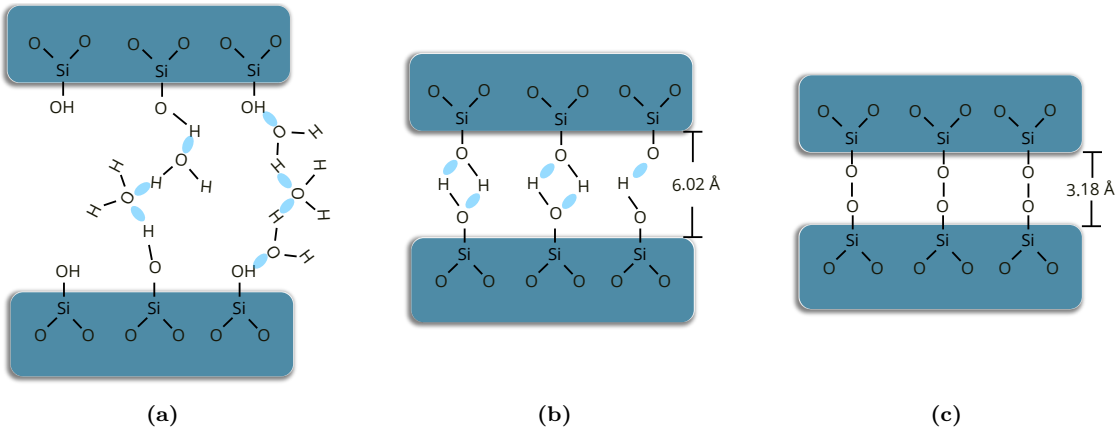

Figure 10. Stages occurring during direct bonding. a) At room temperature (RT)−110°C. b) At 110°C – 150°C water molecules diffuse away. c) At 150°C – 800°C the hydroxyl groups in in close contact form covalent bonds. Adapted from John Wiley and Sons [66].

4 Fabrication

The aim was to produce 30 µm deep channels in a cost and time efficient way. The channels would also need to be smooth and defect free to prevent leaking. To have an efficient development process, chips were manufactured in batches of four to account for possible mistakes. At first, every fabrication step was tested on chips without drilled inlets and outlets to save time while perfecting the process. The aim was to reproduce the process developed in Dr. Ján Borovský's thesis on sorting of carbon nanotubes, which was the further developed by Suha Öcal to better suit for deeper etching [19, 67]. The fabrication steps required a dust free environment, hence they were performed in an ISO5 clean room. As substrate, Menzel-Gläser $20 \times 20 \times 1\text{mm}^3$ microscope coverslips consisting of soda-lime glass were used. The chips were drilled trough with Lambda-Physik OPTex KrF excimer laser to form the inlets and outlets with roughly 100 µm diameter.

Instrumentation:

For evaporation, Balzers Baltec BAE 250 e-beam evaporator was used at a vacuum of (1-2) $\cdot 10^{-5}$mTorr. As SEM for EBL, Raith e-Line was used together with its proprietary software (NANOSUITE, release 6), which includes a CAD tool for layout designing. For plasma cleaning, surface activation and etching (RIE) Oxford Instruments Plasmalab80Plus was used. Optical imaging of the samples was done by Olympus BX51M together with Q Imaging MicroPublisher 5.0 RTV camera. Chemical processes were conducted in fume hoods and spin-coating in laminar flow-hoods. A Laurell WS-650MZ-23NPPB spinner was used for spin coating. To determine surface roughness and channel depth a KLA Tencor P-15 profilometer was used. The chemicals used are presented in Appendix A.

4.1 Design

The chip layout was designed using the electron microscopes own software, Nanosuite. There were two main considerations for the design; The important features required for the chip operation needed to be implemented and it needed to be simplistic, allowing a reasonable exposure time. When developing the fabrication steps, it is important that all the features required can be produced once the fabrication steps are mastered. The most important features were the channels with depth ranging between $(2 - 40)$ µm, width of $(10 - 120)$ µm and the manufacture of electrodes as close as possible to the channels. E-beam was chosen as the lithography method for development to allow fast changes in design if necessary, without the need to create new masks as in photolithography. E-beam exposure time increases with area exposed, which had to be minimized for efficient development.

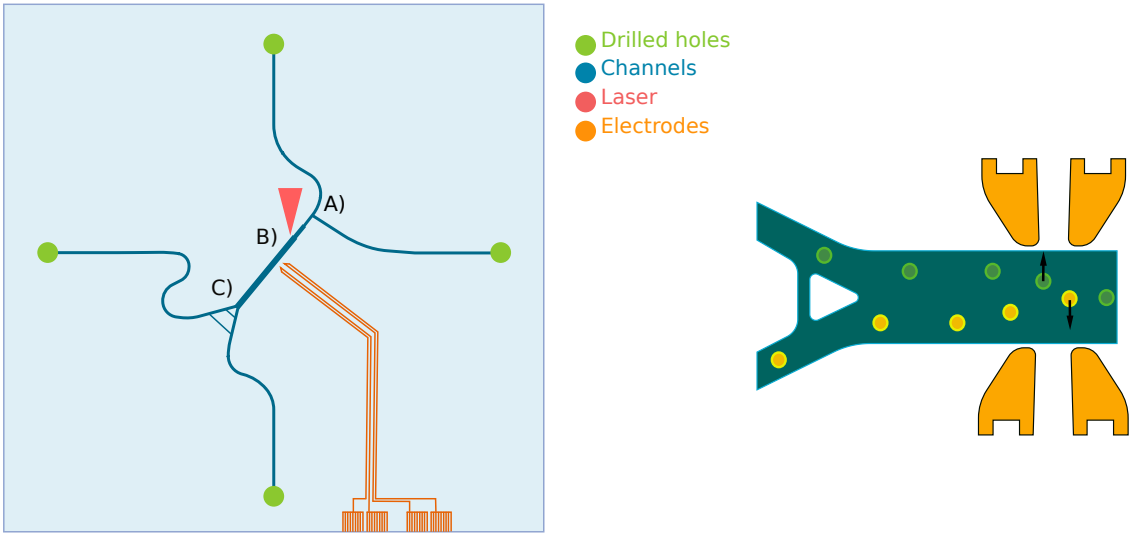

(a) Chip layout.

(b) Deflection of cells to different lanes

Figure 11. The design for the layout of the microfluidic chip.

The three most important areas of the channel layout are visualised in Figure 11a. A) The channels from the two inlets meet at a T-crossing. It allows droplet formation, if droplet-based sorting is to be used, or flow control. If cells are inserted from one of the inlets, the space/medium between the cells can be altered by tuning the second inlet pressure. This flow adds medium in between the cells thus increasing the distance between them. B) Is a narrow channel confining the cells for analysis, which is then expanding into a long and wide channel. In the wider part the flow would slow down due to higher volume and the electrodes placed next to the channel

would push or pull the cells based on their fluorescence. Assuming a laminar flow, the cells would then take the correct "lane" in the wide channel. C) At the Y-junction the cells would go left or right depending on their "lane" to be collected or to become waste (Figure 11b). The junction would also require small channels where cells don't fit across to stabilize pressure. Otherwise a cell going in the right channel would then increase the drag on the fluid, thus causing the left channel to be more favourable for the next incoming cell independent of its lane.

The layout was designed for a chip of 20×20 mm, where the two inlets and two outlets were each 7 mm from the chips centre point (Figure 11a). The channels were designed to curve smoothly without rough edges and shapes to uphold laminar flow and reduce clogging. The channel width was 30 µm for the transport of cells and 5 µm for the pressure stabilizing channels. At the electrodes, the channel width was up to 50 µm to allow proper flow lanes for the cells. The design needed to accommodate for isotropic etching, meaning the channels were always wider than the exposed width. Knowing the correct width was critical in placing the electrodes as close as possible. Concerning the length, the straight part in front of the electrodes needs to be long enough for the spectroscopy and the separation to take place. The inlet channels before the T-junction and the outlet channels after the Y-junction were designed to have matching lengths. Especially for the outlets it is essential because otherwise there would be a pressure difference that would make one channel more favourable for the flow.

The design for the electrodes were reproduced from Borovský's thesis [19]. The tip shape originated from a paper, where the electric fields were simulated to produce an ideal electric field for contactless DEP [68]. The electrodes consisted of a half loop having contact pads at the end for allowing the test whether they were functional. The contact pads were split into vertical lines to reduce the exposure area and thus processing time significantly. The final optimal design would include uniform contact pads and four electrodes. If same frequency pushing or pulling force is to be achieved there need to be electrodes on both sides of the channel. For the process development only two electrodes were manufactured.

4.2 Channels

4.2.1 Initial fabrication

For etch mask deposition, the chips needed to be contaminant free. Glass residue and leftover protective tape from drilling were removed by mechanical scrubbing and hot acetone. The chips were then rinsed with IPA and dried with N_2 gun. To thoroughly clean organic residue and to activate the glass surface, a piranha clean was performed. The piranha solution was made from 3:1 Sulphuric acid and hydrogen peroxide and kept at 100°C for 40 minutes. When done, the chips were dipped into dH_2O for rinsing off any Piranha residues. A layer of 50 nm Cr and 200 nm Au was then evaporated at a rate of 1,0 Å/ sec. After evaporation, PMMA 950K A4 was spin coated at 3000 rpm and prebaked at 160°C for 2 min. A test pattern layout, containing traps and channel intersections was then exposed using EBL with 215 µC/cm^2, developed in MIBK:IPA for 45s and stopped in IPA. The resist was then hard baked at 200°C for 2h on a hot plate. The gold layer was then etched using Gold etchant (Appendix A) for 15s and Cr using Nichrome etchant (Appendix A) for 10s. The glass was then etched with 48%HF (Appendix A) for 1 min. Finally, the resist was removed with acetone and both Cr and Au masks etched away completely with their corresponding etchants.

The result was poor and barely enough for an operational chip. The channel surfaces were rough, and the chip was filled with pinholes (Figure 12). The mask was also in poor condition, containing a lot of pinholes and occasional blister like features underneath. The adhesion of the mask to the substrate was weak which was obvious from mask detachment during sonification. Fixing these issues was not trivial, because the process consisted of many fabrication steps and it was unknown what was the exact cause of these defects. It also took time to master basic cleanroom procedures like precise tweezer handling to minimize mechanically caused defects to the chips.

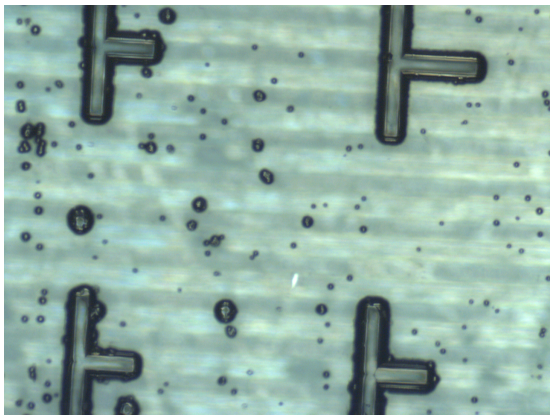

(a) Pinholes

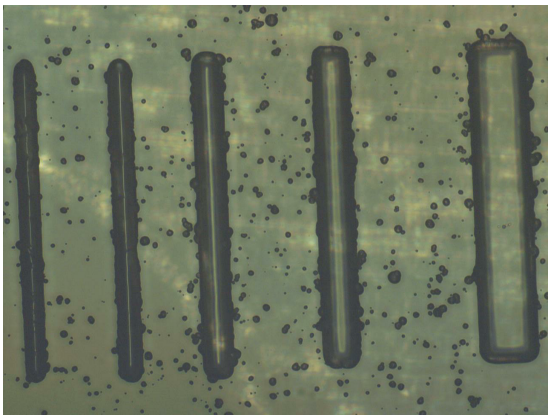

(b) Pinholes

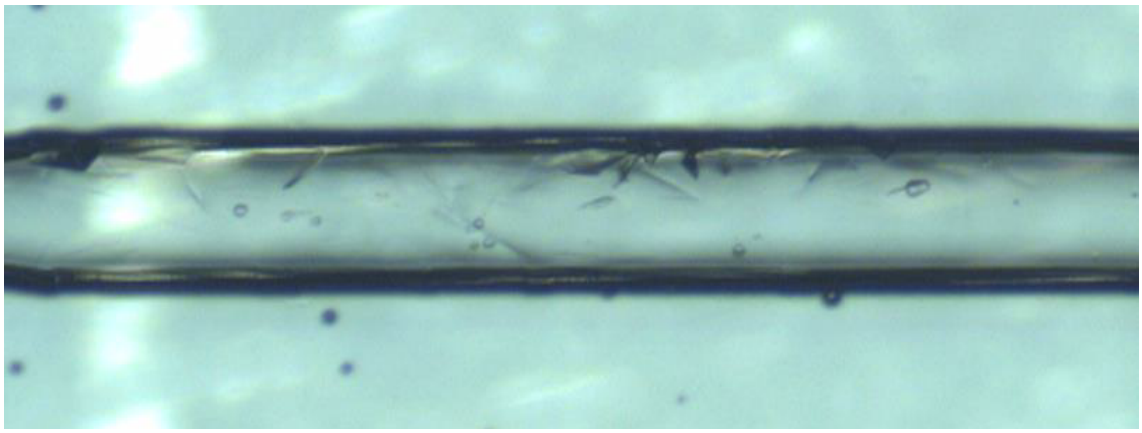

(c) Channel roughness

Figure 12. Optical images of the defects present in the initial fabrication.

4.2.2 Troubleshooting

Channel roughness

The channel roughness was addressed first. It seemed to have a sort of randomness, some chips having smoother channels than others. Although, it did appear more consistently in thinner channels (5 µm in design) and was almost non-existent in wide areas (over 30 µm in design). After a thorough literature search, it was obvious that soda-lime glass forms insoluble products with HF. The impurities (CaO, Al_2O_3, MgO) present in soda lime will form precipitates [51, 53]:

$$CaO \rightarrow CaF_2,\ MgO \rightarrow MgF,\ Al_2O_3 \rightarrow AlF_3$$

By adding HCl into the etchant, these products can be made soluble:

$$CaF_2 \rightarrow CaCl_2,\ MgF \rightarrow MgCl_2,\ AlF_3 \rightarrow AlCl_3$$

Iliescu et al. (2005) found the optimal ratio for HF:HCl to be 10:1 concerning

surface roughness and etch rate [53]. Due to practical convenience (beaker size) 48 % HF was mixed with 37 % HCl (Appendix A) in a ratio 9:1 (18 ml : 2 ml). This caused a significant improvement in surface roughness. These roughness defects were still present in the thinner channels and at the outlines of the channels that were isotopically etched under the mask. This is probably a result from fresh etchant not being able to reach small corners and areas as efficiently, thus the mixing of the insoluble products with the bulk solution was slowed. Gentle mixing was applied during HF-etching to overcome the problem. The gentle wiggling of the chip during etching did yield better results but to totally overcome the problem sonication would be required. Sonication was not applied due to safety reasons of the toxic HF.

Mask quality

To fix the mask quality to an acceptable level, almost every fabrication step had to be slightly improved. The two main reasons for bad mask quality were contaminated substrate surface and poor evaporation quality. To improve the cleanliness of the surface, scrubbing and sonication in acetone was repeated multiple times. Sonication and rinse in IPA were also applied. The chips were then checked against light to see whether all visible contaminants have been removed. The chips were put in a flat beaker in dH_2O to avoid any contamination from ambient air while transporting them between fabrication steps. To improve the film adhesion the activation step was altered. Different Piranha (H_2SO_4:H_2O_2) mixtures ranging between 2:1 and 5:1 were tried with varying activation times (30 min to 1 h), but they did not alter the outcome on an observable level. The piranha treatment was altered to last 30 min, then a thorough rinse (over 30 s) in dH_2O and putting it back to the piranha (cool) solution for 10 min. The chips were then again thoroughly rinsed and put in dH_2O. This was done to increase the density of hydroxyl groups on the surface and to rinse any contaminants. Careless cleaning of piranha residues from the chip leads to disastrous results (Figure 13a). Prior to evaporation the chips were put on a hotplate at 130 °C for 2 min to evaporate all moisture. Higher temperatures were avoided to minimise desorption of the hydroxyl groups.

A set of challenges were faced with the evaporator. Electrical contact problems were randomly present causing difficulties on setting a constant evaporation speed (Figure 13b). Contact problems also caused current spikes that hit the crucible, thus evaporating crucible material and causing film contamination. The evaporator

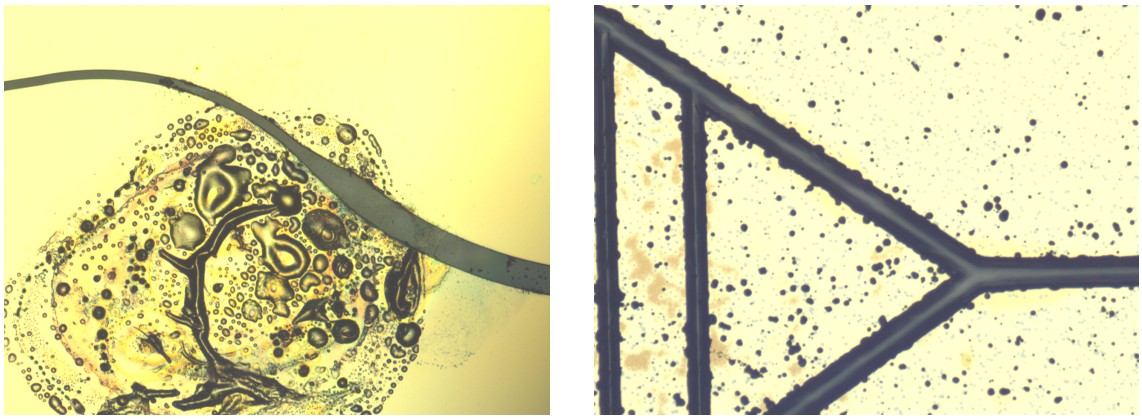

(a) (b)

Figure 13. a) Piranha residue under mask layer. Only visible after evaporation. b) Bad mask quality due to failed evaporation.

being under constant use, various evaporation materials had accumulated around the crucible. By distorting the magnetic field, this led to the electrons missing the target material and hitting the crucible. Cleaning of the evaporator and sonication of the target material and the crucible in IPA before evaporation, had a noticeable positive effect. The target Cr was also changed to fresh unoxidized pellets and there-on kept in N_2 atmosphere cupboard to avoid oxidation.

Consequently, the number of pinholes were reduced but not completely eliminated. Multiple researches suggest having a double layer of gold to reduce pinholes [56, 55, 69]. The idea is that when pinholes are generated from contamination particles or the stress of the film, they will be generated randomly. Depositing a second layer on top, that will also have defects randomly, the second layer would mostly cover the pinholes generated in the first layer. Between the depositions the film would be cooled and the defects generated due to tensile stress (Figure 14). Combinations of 70 nm + 70 nm + 70 nm, 150 nm + 150 nm and 200 nm + 100 nm Au layers were tried. The triple 70 nm layer was weak with a lot of pinholes with the top layer detaching just from sonication. The 200 nm + 100 nm Au with waiting 15 min between depositions yielded a very positive result, thus it was kept as the method for further development.

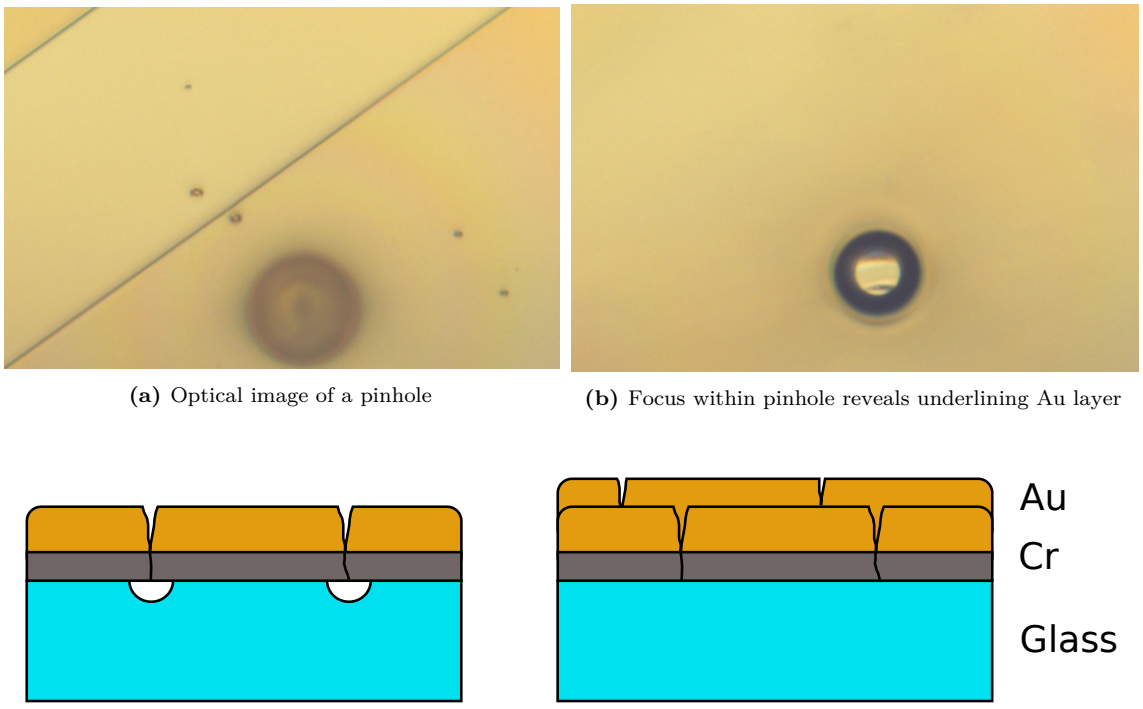

(a) Optical image of a pinhole

(b) Focus within pinhole reveals underlining Au layer

(c) Double layer Au mask

Figure 14. The double layered Au mask. When a pinhole is generated in the top layer, the underlining layer can still be intact and protect the sample.

Channels etch

To get the right channel depth, the etch rate of the HF:HCl solution was determined. The channel depth and profile for various etching times were measured with a Profilometer and it was found to be 0,55 $\frac{\mu m}{s}$ (Figure 15). The isotropy of the etch profile was important in placing the electrodes close to the channels (Figure 16). The lateral etch rate was found to be the same as the vertical rate.

The only requirement for embedding the electrodes within the chip was the electrode-channel being deeper than the electrode thickness (over 170 nm). Because high lateral precision was not required, a HF dip was deployed using only PMMA as mask. With the absence of a metal mask, the charging of the sample during EBL was solved using a conductive resist on top (Electra 92, Appendix A). It is water soluble, meaning that it can be removed before development by dipping in dH_2O and the hydrophobic PMMA will go unaltered. Dipping times of 1,5 s and 10 s with concentrations of HF (48% and 20%) were tested, all leading to failure. The resists didn't get destroyed but it peeled off from the glass. PMMA is resistant to HF but the adhesion layer between glass and PMMA is not. Its adhesion to glass results

from its the basic carbonyl groups and the acidic silanol (Si-OH) groups on glass surface [70]. Either by diffusing through PMMA or between the interface, HF will react with the hydroxyl groups and detach the resist from the glass. In order to improve the adhesion, a 100 nm Cr layer was used as etch mask under the PMMA. With hardbaking the resist, the Cr mask proved sufficient for shallow channel etching (etch time 2s).

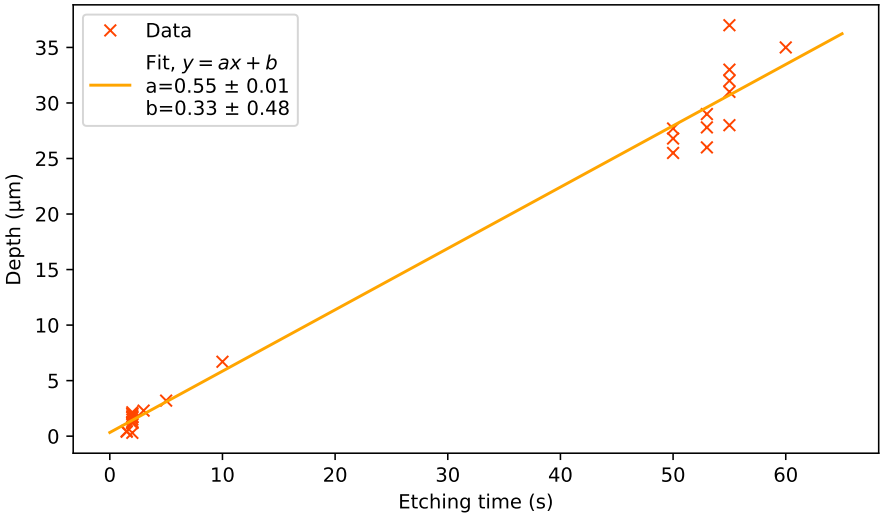

Figure 15. Etch rate of soda-lime with HF:HCl 10:1. The rate variation is a result of differing channel width. A depth variation up to ±5 µm was measured for channels, wide ones being deeper and vice versa.

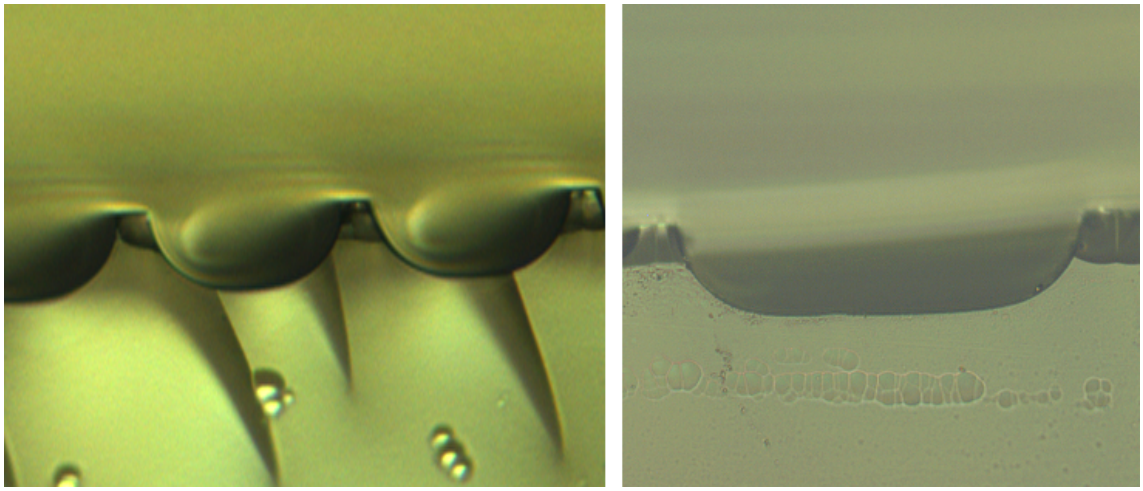

Figure 16. The etch profiles of channels with mask openings of 10 µm (left) and 50 µm (right) taken with an optical microscope.

4.3 Electrodes

The electrodes were fabricated to meet the requirements of contactless DEP. This means that they need to be as close possible to the microfluidic channels, but avoiding contact. Because of the 1 mm thickness of the chip and the cover glass, the electrodes should be placed in between the glasses. Due to the low surface roughness requirement set by TADB the electrodes cannot be placed between the glasses without immersing them into the glass. For proper bonding, an average surface roughness of 50 nm is allowed [65]. Depositing electrodes (over 170 nm thick) directly on glass surface, would create newton rings and their location next to the channels would cause leakage.

Fabrication

The first decision in electrode fabrication was whether to do it before or after the etching of the main channels. Etching the electrode-channels together with the main channels holds many advantages. Not needing to do a second lithography process (including activation, mask evaporation, exposure etching) would save in time and cost. Reducing the fabrication steps guarantees a higher success rate for a working chip fabrication. Furthermore, etching only once would reduce the amount of pinholes. Simultaneous etching meant that the electrode channels would be at the same depth as the main channels. This caused a challenge for protecting the main channels during electrode deposition. The bad step coverage of PMMA leads to unprotected edges (Figure 17). Multiple layers of PMMA were spun as a protective layer, but the steep edges were always left unprotected. A sandwich of PMMA-Cr-PMMA was also tested, but during prebake, the Cr-layer cracked becoming useless. As a last resort, protection of the channels with tape was tried, but it was not suitable for the high precision requirement of the electrode-channel distance.

Arguably, the problem of covering properly the 30 µm deep channels could have been solved using a photoresist and photolithography or by spray coating PMMA to have ideal step coverage. These methods not being readily available at the facility, the second option was chosen, which was to manufacture the electrodes first. Fabricating the electrodes first meant that they need to be capable of withstanding the etching of the deep main-channels and the removal of the Cr-Au mask. Shallow (1-2 µm) deep channels were etched for the electrodes using a 100 nm chromium

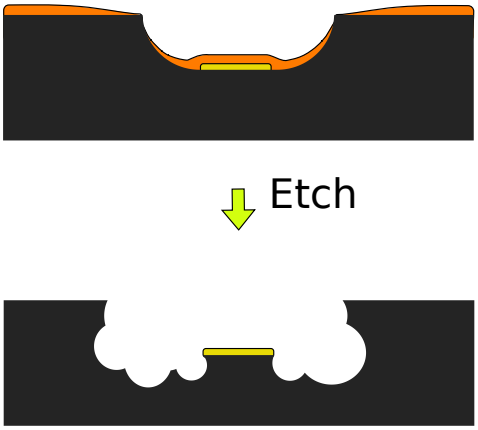

(a) PMMA step coverage

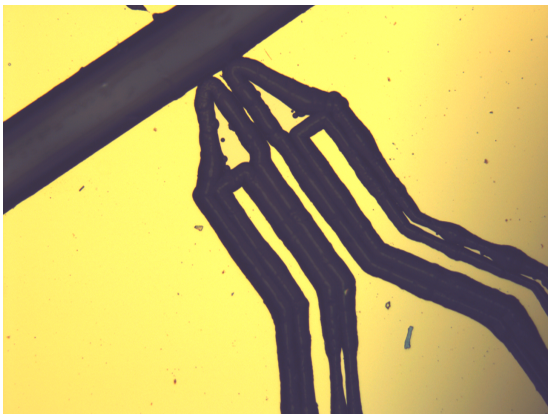

(b) Unwanted etching of sharp features

Figure 17. Using a PMMA layer thinner than electrode depth or not evaporating at an angle will cause sharp edges to be etched.

mask. The electrode material could be then deposited without removing the etch mask. This meant that the electrode material had a "double lift-off" by the removal of the resist and the Cr-mask. It made sure that no unwanted electrode material was left on the surface. The shallow depth also allowed the use of PMMA. Spin coating PMMA A11 at 3000 rpm results in a thickness of 2,25 µm, which grants complete coverage of the electrodes. Evaporation of the deep-etch Cr/Au mask at 45° with wafer rotation ensured mask coverage as well.

For the removal of the Cr-mask, a Nichrome etchant was used. Its selectivity was ideal; not harming the electrodes in any way [49]. This property was also exploited for the removal of the deep-etch mask. On top of the electrodes a Cr-Au was evaporated. After etching, the mask could be removed by using solely the Nichrome etchant. Using a gold etchant could have harmed the electrodes which contained gold.

The "lift-off" of the gold mask happened a lot faster (5 min) than expected from the etch rate of nichrome etchant ($50\,\frac{\text{Å}}{\text{s}}$ at 40 °C). It was expected to last a long time, considering the large area of 20×20 mm. This is speculated due to an electrochemical effect between the Au/Cr interface and the etchant solution, which has been demonstrated by Nemirovsky et al. for undercutting of Au when iodine etchants are used. Although in this case beneficial, the fast under etching of the Cr layer caused destruction of the electrodes in a few experiments (Figure 18). Another reason could be the stress within the deposited gold film. The tensile lifting the gold could lead to the detachment and peeling of either the Au/Cr or the Cr/glass interface allowing the Cr-etchant to etch the underlying chromium (Figure 18).

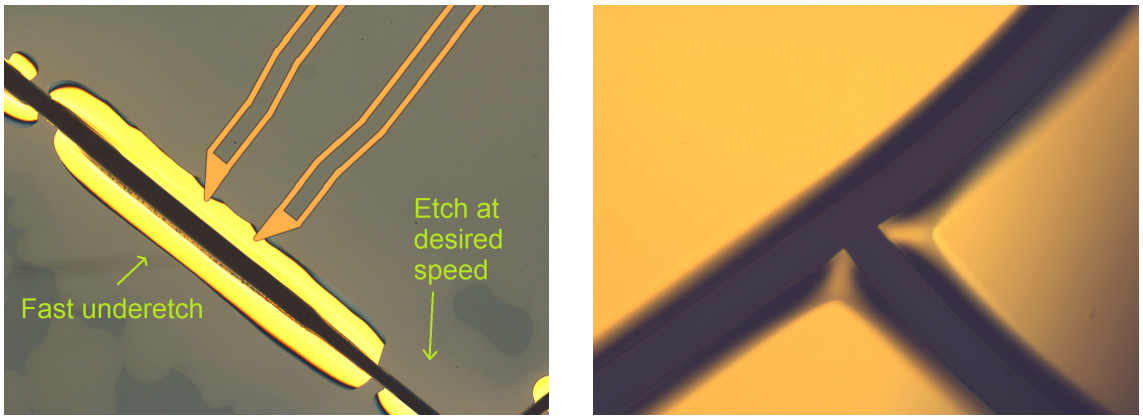

(a) (b)

Figure 18. Over etching of Cr under Au mask. a) The fast under etching of Cr ruined the electrodes. (Image taken from the bottom of the chip) b) Tensile stress visible when the gold mask is peeling upwards after channel etch.

Composition

Besides good conductivity, the requirements for the electrode composition arise from the chip fabrication steps. The electrodes need to withstand:

I The etchants used in lift-off

II Good adhesion to glass, for cleaning steps (sonication)

III Can endure Piranha treatment for chip activation (for TADB)

IV Thermal endurance; not melting and retaining conductivity after being subjected for 590°C in TADB

V Can be soldered to connecting wires

An electrode composition meeting the requirements had already been demonstrated by Borovsky [19]; It was a sandwich of SiO_2, Ti, Au, Ti and SiO_2. Gold was chosen because its ideal conductivity and chemical resistance. As an adhesion layer between gold and glass, titanium was chosen. Although Ti is a slightly weaker adhesion layer than Cr [44], the annealing temperature in TADB causes chromium to diffuse into gold increasing its resistance significantly [71]. Titanium will also diffuse through Gold forming $TiAu_2$, TiAu and Ti_3Au compounds. The Ti_3Au forms a thin (50−100 Å) diffusion barrier preventing further diffusion [72]. The initial SiO_2 layer was designed to prevent diffusion between Ti and Glass which would lead to defective electrodes. The first SiO_2 layer was deemed unnecessary and working electrodes were manufactured without it. Adhesion problems between the deposited SiO_2 and

the electrodes drove towards this decision (Figure 19). It can be speculated that the first SiO_2 layer is indeed mandatory if the electrodes are placed between glass slides and subjected to pressure. The pressure may have lead to melting point depression and increased diffusion, which was not the case with our embedded electrodes. After TADB a slight change in electrode colour was observed but the electrode resistance (800 Ω to 1 kΩ) was not affected.

(a) **(b)**

Figure 19. a) Electrodes detaching from glass due to bad adhesion. b) HF etched the protective SiO_2 layer through a pinhole, which lead to piranha corroding the gold.

To further improve adhesion and to avoid Ti oxidation, all of the electrode materials were evaporated consecutively. The final layer (SiO_2), which served a purpose of protecting the electrodes against Piranha treatment (Figure 19), made the electrode surface non-conductive. As a final processing g step after cover-glass bonding, this layer was etched away using a RIE oxide etch. This etch did not visibly alter the glass cover transparency. To summarise, the final composition of the electrodes is displayed in Table 3.

Table 3. The final electrode composition.

Order	Material	Thickness	Purpose
(1)	Ti	10 nm	An adhesion layer between Glass and Gold
(2)	Au	50 nm	A long lasting and chemically resistive conductor
(3)	Ti	10 nm	An adhesion layer between Gold and the protective layer of Silicon dioxide
(4)	SiO_2	100 nm	Acts as a protective layer against corrosive chemical treatments and separates electrodes from masking metal films

4.4 Experiment setup

The aim of the experimental setup was to observe whether the deflection of cells using DEP is successful. For the setup a custom-made chip holder was used with four tubes acting as inlets and outlets. The connections between the tubes and the chip itself were secured by Viton rubber O-rings to prevent leakage. A pressure driven flow was achieved by connecting the inlet tubes to a Fluigent MFCS-EZ pressure controlling device, which was driven by N_2 flow capable of producing up to 2 bars of pressure. To model fluorescing cancer cells, SPHERO^{TM} Fluorescent Yellow Particles (FP-6052-2) with a size of 5.0-7.9 µm and an excitation and emission spectra of 430-480 nm, 470-520 nm. These particles consist of polystyrene cores that are covered with fluorophores. The beads original concentration of 1% w/v was diluted 1/10 in 10^{-4} % Tween-20®, which is a Surfact-Amps Detergent. The detergent molecules, having a hydrophilic "tail" and a hydrophobic "head", make the fluorescent beads hydrophilic and thus water soluble (acting like soap), otherwise they would aggregate and resist resist mixing with water. The setup is displayed in Figure 20.

To connect the chip to a DEP source, thin wires were soldered to the electrodes using indium. It was chosen as a solder due to its low melting point (156°C), its ability to adhere to glass and the fact that tin-based solders can scavenge gold and ruin the electrodes. Through the soldered wires the conductivity of the electrodes could easily be confirmed. To produce the electric fields for DEP, a KEITHLEY 2410-c high voltage generator was connected to a custom-made signal generator circuit that was controlled by an Arduino. The Arduino allowed the controlling of the signal frequency (up to 30 kHz) and the pulse amount. The circuit, displayed in Figure 21, was slightly modified from the original one created by Ján Borovsky to allow usage of smaller currents.

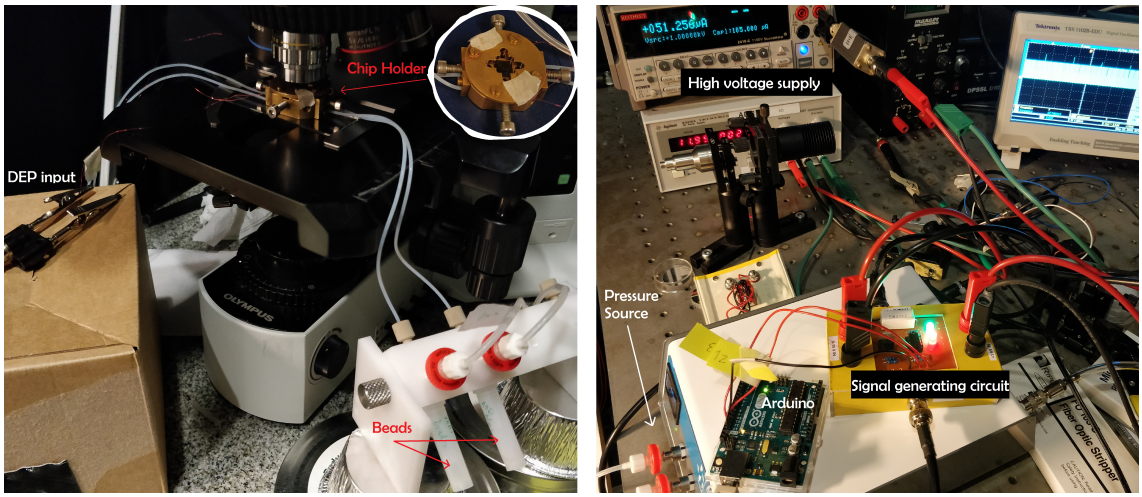

Figure 20. Setup under a microscope to detect DEP sorting of fluorescent beads.

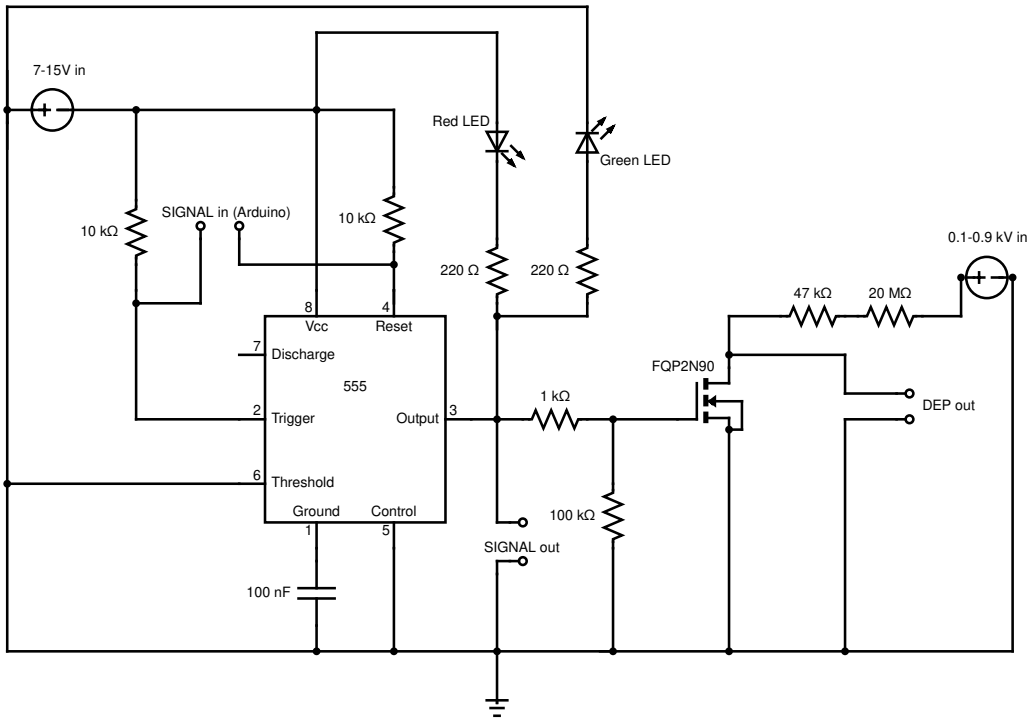

Figure 21. The schematic of the circuit used to generate DEP signal.

5 Results and discussion.

5.1 Fabrication of the chip

After numerous trials and errors, eventually a successful chip with smooth channels, correct channel depth and working electrodes was manufactured. A significant improvement in etch-mask and channel quality was achieved compared to the initial fabrication experiment. The resulting smooth channel surface and the lack of pinholes can bee seen in Figure 22.

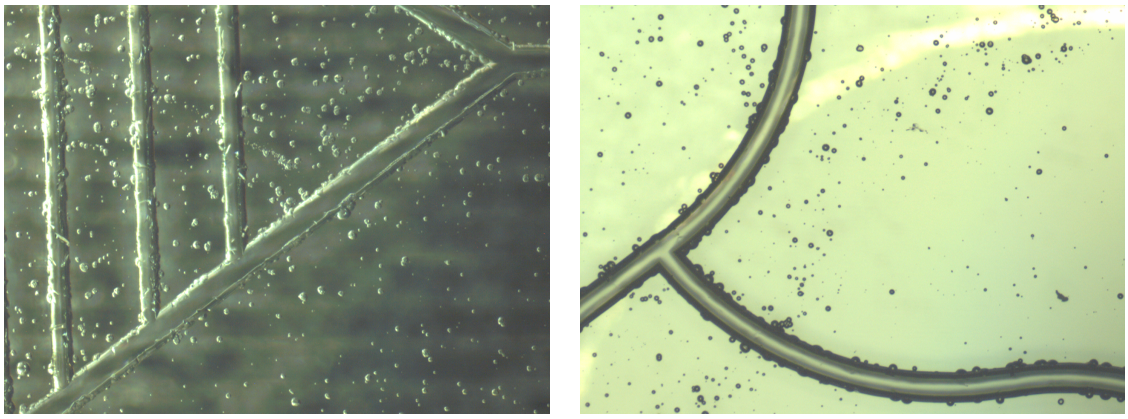

(a) Poor fabrication results.

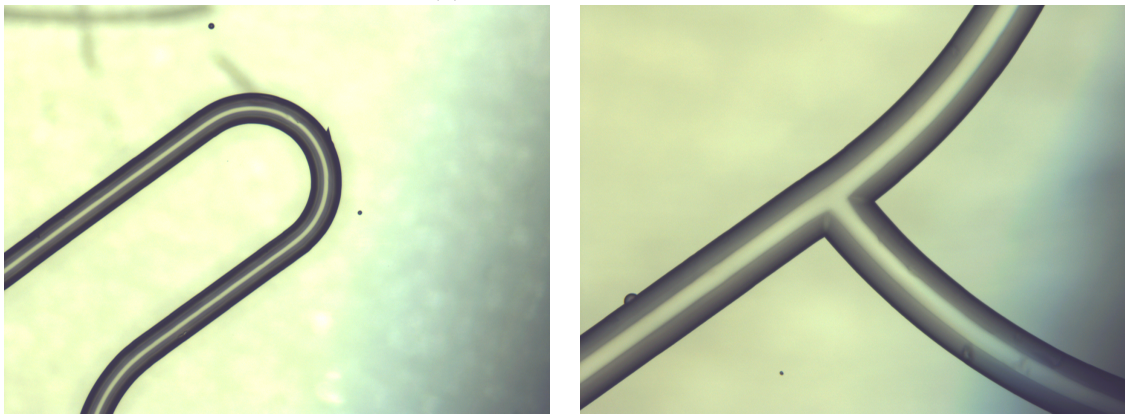

(b) Optimal results after developed fabrication steps.

Figure 22. Optical images of the chips surface before (a) and after (b) the development and optimization of the fabrication steps. The amount of pinholes were reduced and channel roughness decreased.

Decreased channel roughness was achieved by annealing the chips after the

inlet/outlet drilling and by adding HCl to the HF etchant in a ratio of 10:1 (HF:HCl). Minimizing channel roughness is important when laminar flow is to be maintained and clogging of the channels avoided. The pinhole density was reduced by improving the cleaning procedure of the chip and by using a multilayer Au mask with a Cr adhesion layer.

Conductive electrodes that could withstand piranha treatment and the annealing temperatures of TADB were successfully fabricated (Figure 23a). The 100 nm of SiO_2 was enough to protect the electrodes from room temperature piranha. Activating the electrode-channels surface by RIE O_2 treatment, the adhesion between glass and titanium was increased which resulted in better endurance to sonication. During TADB the electrodes experienced a slight colour change to a slightly darker tone, which might result from Ti diffusion to Au, but no change in conductivity was observed. The only complication left in electrode-fabrication was the formation of blisters days after deposition, but before TADB annealing. The blisters were observed to be between the Ti and the Au layers, the bottom Ti layer still adhering to glass while the top layers delaminating (Figure 23b). This is probably due to tensile stress resulting from gold having a higher thermal expansion coefficient than the Ti layer. These defects might start from impurities deposited during evaporation, which reduce the adhesion between the bottom Ti and Au layers. The blisters did not cause complications when annealing or for conductivity, but sonication while blisters are visible resulted in destruction of the electrode.

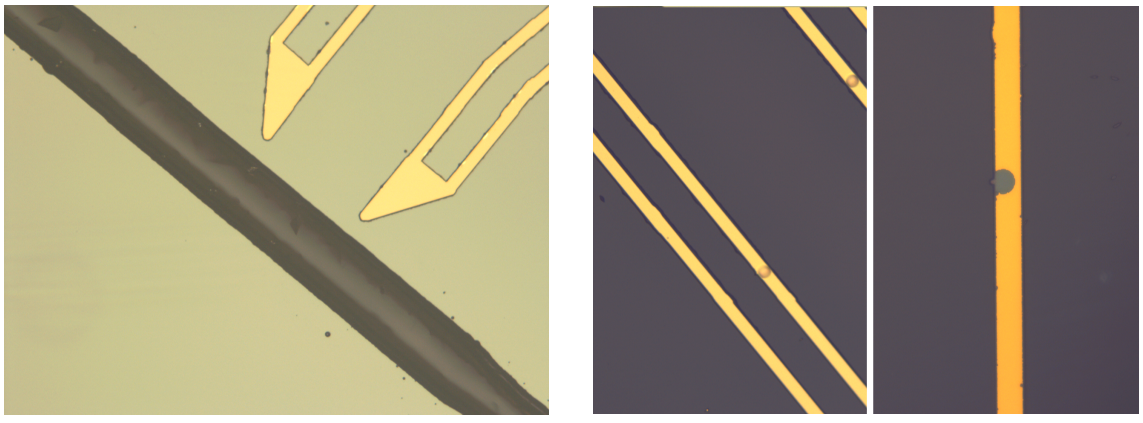

(a) (b)

Figure 23. a) Image of a successfully fabricated electrode. b) Blisters formed on electrodes (left) that will detach if sonicated (right).

5.2 Overview of the process

Here the complete realisation of the working microfluidic chip is presented. A more precise recipe is presented in appendix B. The fabrication steps for a successful chip are shown in Figure 24.

1) Soda Lime-glass microscope coverslips are used as substrate, with holes with a diameter of 100 µm for inlets and outlets drilled prior to the cleanroom processing. The glass chip is cleaned and treated with Piranha-solution prior to thin film deposition.

2) Using E-beam evaporation, a of 100 nm Cr thin film is evaporated to act as an etch mask. Next, PMMA of about 250 nm is spun before e-beam exposure.

3) The electrode design is then exposed with electron beam lithography and developed.

4) The Cr-mask is etched followed by a dip into HF-HCl (10:1) solution to etch shallow grooves for the electrodes. After etching, a RIE O_2 etch is used to activate the glass and clean etching residue from electrode channels.

5) Electrodes are then evaporated; a metal sandwich of 10 nm Ti +50 nm Au +10 nm Ti +100 nm SiO_2).

6) Lift-off is then carried out and the Cr-mask etched away.

7) A tougher RIE O_2 treatment is used to activate the glass surface and 50 nm Cr + (150 + 150) nm Au is evaporated in an 45° angle while the wafer is rotated ensuring deposition to the walls of the trenches.

8) Now 2,2 µm of PMMA is spun to cover the shallow channels of the electrodes completely.

9) Alignment, exposure, and development of the Channels-layout is performed.

10) The Au and Cr masks are etched followed by a 55s HF-HCl etch of the channels. After removing the e-beam resist the gold mask is removed by etching the underlining Cr.

11) Finally, the chip and its cover are cleaned and activated in Piranha so it can be bonded. The bonding is performed in a furnace at 585 °C for 2h. The bonded chip is then treated with a RIE oxide etch to reveal the electrode pads for soldering and the chip is ready.

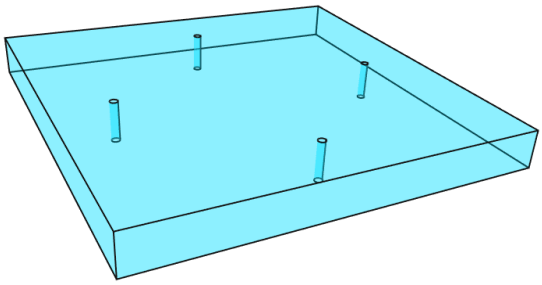

(1) Drilled Soda-lime glass chip

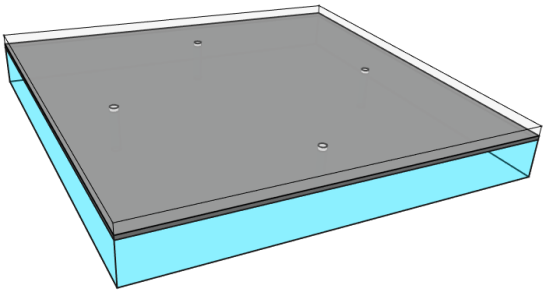

(2) 100 nm Cr + 250 nm PMMA

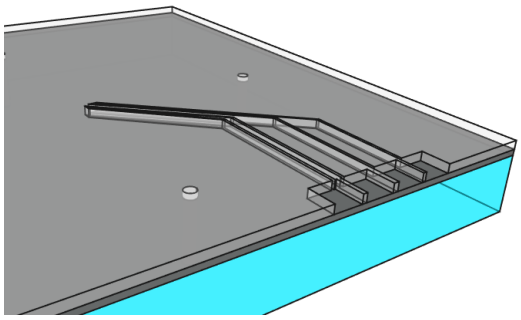

(3) PMMA exposed and developed

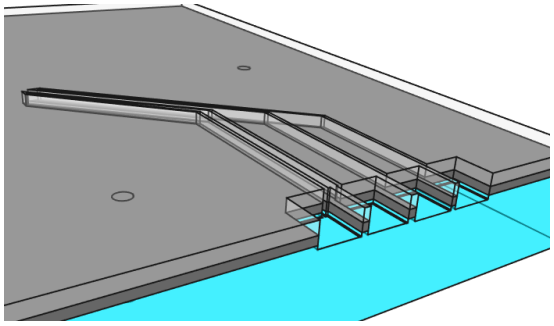

(4) Cr-mask and Glass etched

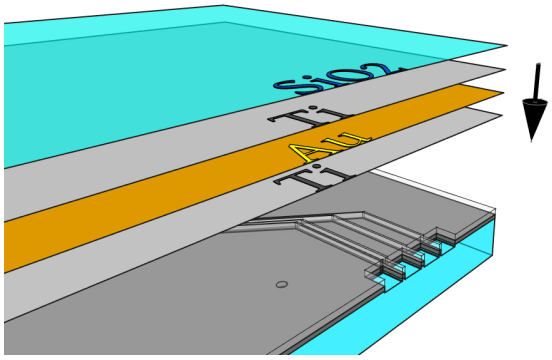

(5) Electrodes deposited (10 nm Ti + 50 nm Au + 10 nm Ti + 100 nm SiO_2)

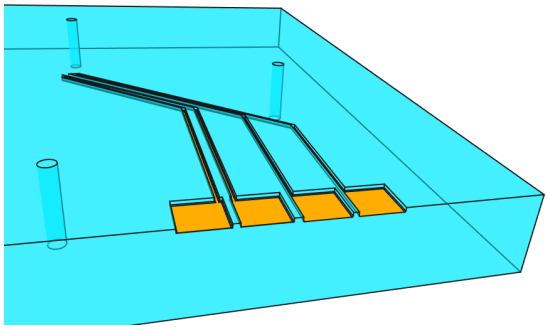

(6) Lift-off and etching Cr

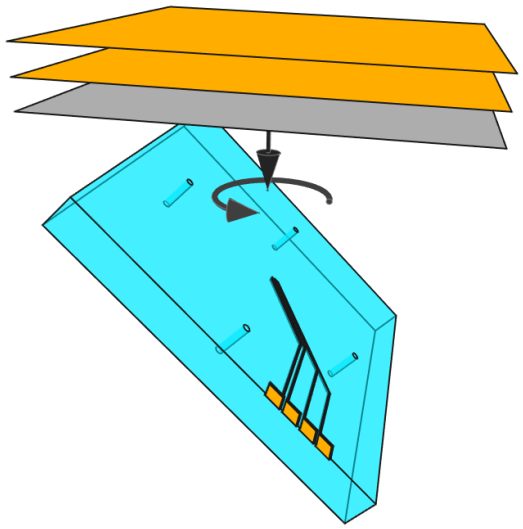

(7) 50 nm Cr + (150 + 150) nm Au deposited at 45° angle on a spinning wafer

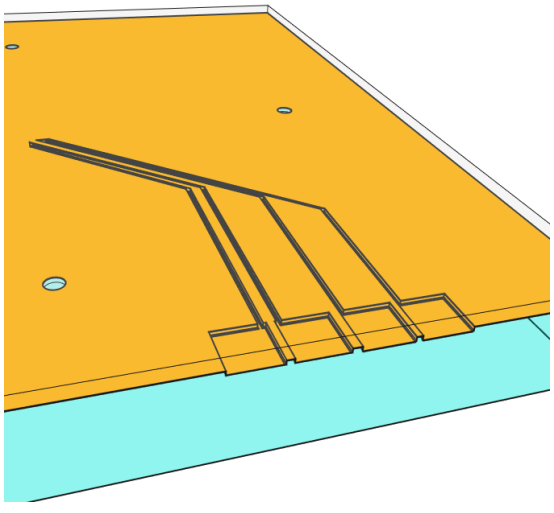

(8) 2,2 µm PMMA

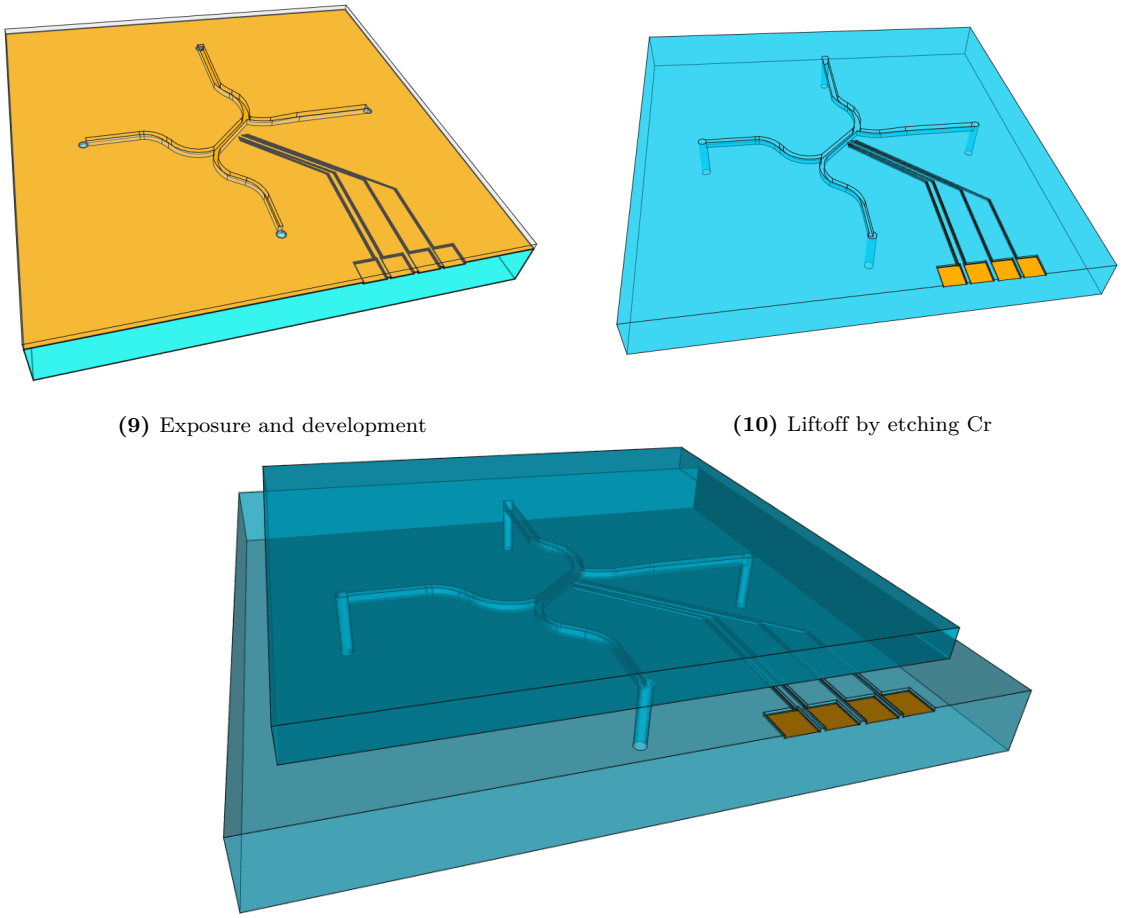

(9) Exposure and development

(10) Liftoff by etching Cr

(11) Thermally bonded cover

Figure 24. The fabrication steps for a functional microfluidic chip

5.3 DEP using fluorescent beads

As the first measurement the flow through the channels was measured. Visible flow of the beads was observed between $3-40$ mbar of pressure, higher pressures requiring a high speed camera due to the velocity of the beads (Figure 25). The huge variation was the result of pressure leaks within the tubes containing the beads and their holder. Because of clogs and gas leakage between the testing tube containing the beads and its holder the exact pressure within the channels remained unclear. Especially after testing with larger $10-14$ µm Fluorescent Nile Red particles, clogging was observed at high (over 50 mbar) pressures. Even though all visible clogs within the channels were removed by injecting bubbles into the tubing using a pipette, clogs remained in the outlet tubes. This was obvious from the pressure difference present in the outlet channels.

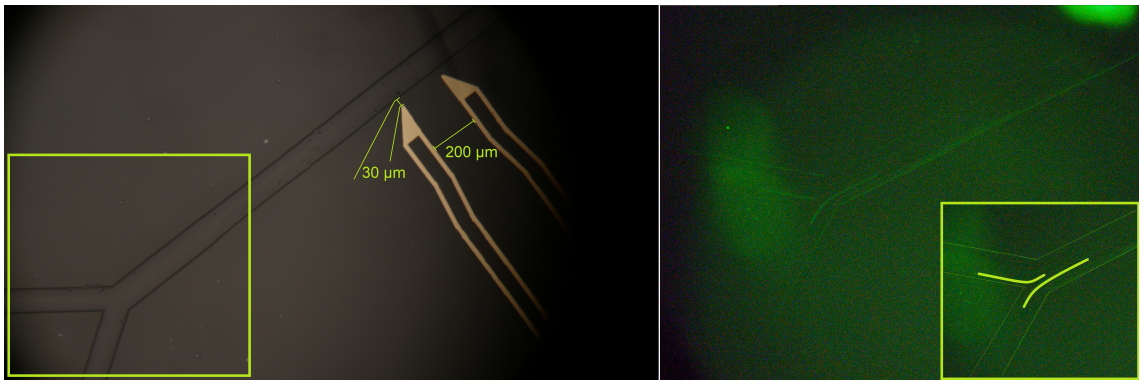

Figure 25. (Left) Operational chip with electrode dimensions. (Right) The green square area imaged through a filter to visualise fluorescent beads flowing to the outlet corresponding to their lane.

Despite having minor problems with pressure control, laminar flow in front of the electrodes was achieved which was sufficient for testing DEP deflection. The laminar flow was obvious from the beads keeping constantly the same "lane" they were travelling and the applicability of a Poiseuille flow due to the beads speed difference based on their distance from the channel edges [Video1, Video2]. When the outlet pressures were similar, the beads travelled into the channel corresponding to their "lane". When testing the effect of DEP, the beads were moved slowly back and forth in front of the electrodes to clearly see whether they experienced any deflection [Video3]. Square waves with a peak to peak voltage of 1 kV were driven through the electrodes at frequencies of 1 kHz, 10 kHz and 30 kHz, without any observable effect on the beads. The main reason is believed to be originating from faulty electrodes. The right electrode was soldered multiple times which likely led to the destruction of the connection pads. Although no current could be measured across the faulty electrode, the tests were still run in hopes that at least one of the two bonding pads could be still operational, which would be enough to generate the necessary electric fields. Tian et al. have demonstrated an electrophoretic microtrap with the same fluorescent particles used in this thesis, electrodes at a 20 µm distance from channel edge and using electrodes at a potential of 700 to -700 V [73]. Although our electrodes were at a 30 µm distance, we are working in the same order of magnitude with dimensions and voltages. In our design the distance between the electrodes was 200 µm to spread the electric field gradient over a larger area (Figure 25). The purpose was to allow the fast travelling particles to experience DEP force over a longer distance compared to a stronger, short distance effect.

To get the deflection of the beads to work the first step would be to manufacture a new chip and successfully solder the connecting wires to the connection pads. Oher troubleshooting ideas would be to redesign the signal generating circuit to produce higher frequencies (up to 100 kHz) with higher voltages (amplitude of 800 V) to increase the DEP Force. Unfortunately, the manufacture of a new chip after the first successful one was not possible due to limited access to the cleanroom as a result of the COVID-19 pandemic.

5.4 Future design improvements

Considering the future development of the chip design and the DEP sorting, multiple improvements can be made. To eliminate the pressure difference at the Y junction, the pressure stabilising channels could be etched together with the electrode-channels (depth 2 µm). This would allow the pressure to stabilise, without letting the particles change their exit route through the pressure stabilising channels. This solution would only require a slightly increased electron beam exposure time with no extra fabrication steps. The etching of shallow channels separately from the main channels allows design improvements for pressure and flow control. Besides pressure stabilising channels, the flow speed could be tuned. At the area of spectroscopic analysis, shallow side-channels separating from and flowing back to the main channel could be etched. The alternative route for the liquid would slow down the flow in the main channel in the desired area, thus creating a "speed trap" and allowing more time for analysis.

To increase the effectiveness of the DEP force, electrodes could be fabricated on both sides of the channels and tune the frequencies such that one side would push and the other pull the particles. To get the electrodes closer to the channel centre, which is limited by the mask adhesion, the channel width could be minimised to a point where sorting is still achieved. Placing the electrodes closer posed the danger of the HF etching the electrodes. Even a small amount of HF breaching the electrode channels will quickly etch the evaporated SiO_2 layer protecting the electrodes. The stress in the mask and the small adhesion area between the electrodes and the channels caused the Cr adhesion layer in the mask to get under etched. Further improving mask adhesion would allow for electrodes to be placed closer and granting a possibility for a stronger DEP force.

6 Conclusions

In this thesis the successful fabrication of a glass microfluidic chip suitable for dielectrophoresis (DEP) and spectroscopy was demonstrated. The chip contained 30 µm deep and 80-170 µm wide channels connecting to laser-drilled inlets and outlets. Thermal assisted direct bonding at 585 °C was utilised to bond a cover glass to the chip, sealing the channels. Electrodes were also imbedded at 2 µm depth at a distance of 30 µm from the channels to allow the utilisation of DEP. To imprint the channel and electrode design, E-beam lithography was used to allow fast alteration of the design.

Many challenges were faced during the fabrication, most of which were solved. Etching defects caused by pinhole generation were minimised by multiple factors. Using a highly concentrated etchant (48 % HF) increased the etch rate resulting in shorter etching time, which consequently reduced the time for defect formation. Reduced exposure to ambient air, an activation step with dH_2O washing between piranha treatments and the maintenance of evaporator cleanliness further reduced pinhole generation. A HF etch mask of 50 nm Cr as adhesion layer with 200 nm + 100 nm of Au on top proved to be durable with little defects. While the first Au layer adhered to the Cr layer and protected the sample from HF etchant, the second Au layer's purpose was to cover the pinholes generated in the first one. Channel roughness was addressed by adding HCl to the HF etchant to remove the insoluble products generated by etching of soda-lime glass.

Gold electrodes were fabricated with Ti adhesion layer both on bottom and top which were then covered with a protective SiO_2 layer. A short RIE O_2 treatment was used after the 2 µm deep electrode-channel etching to improve adhesion. The electrodes were durable enough to withstand sonication, piranha treatment and the high temperatures of TADB. The slight depth of the electrode channels enabled protection against 1 min of HF etching by using a mask evaporated at an angle and PMMA. After the cover was bonded to the chip, the protective layer was etched from the electrode contact pads using RIE.

The fabrication parameters for all the necessary elements required in a microfluidic chip capable of DEP sorting were optimized and a cook-book was created (Appendix

B). The design was created with fast development of the fabrication steps in mind. Improvements such as the addition of more electrodes and pressure stabilising channels should be considered when fabricating an operating chip.

The first successfully manufactured chip was tested with driving fluorescent beads through the channels. There were no observable leaks from the channels and laminar flow was achieved. Deflection of the beads with a peak to peak voltage of 1 kV and frequencies between 1-30 kHz was attempted with no measurable result, most likely due to a faulty contact pad soldering. Further experimentation and fabrication of a new chip with the already established recipe was not possible due to the COVID-19 pandemic.

Altogether, the developed fabrication recipe and the setup for testing grants a basis for future experiments. Once DEP is achieved, testing with living cells should be initiated. Development of the design would be easy and fast due to the utilisation of E-beam lithography. The glass chips allow for high pressures (over 2 bars) and transparency for high speed sorting using spectroscopy to differentiate between cells. Such a device would have a significant impact on cancer research and through the capability of sorting metastatic cancer cells directly from blood at a high frequency.

References

[1] L. Gervais, N. De Rooij, and E. Delamarche. "Microfluidic chips for point-of-care immunodiagnostics". In: *Advanced materials* 23.24 (2011), H151–H176.

[2] G. M. Whitesides. "The origins and the future of microfluidics". In: *Nature* 442.7101 (2006), pp. 368–373.

[3] C. Huang et al. "Enrichment of prostate cancer cells from blood cells with a hybrid dielectrophoresis and immunocapture microfluidic system". In: *Biomedical microdevices* 15.6 (2013), pp. 941–948.

[4] J. Voldman. "Electrical forces for microscale cell manipulation". In: *Annu. Rev. Biomed. Eng.* 8 (2006), pp. 425–454.

[5] K. Ahn et al. "Dielectrophoretic manipulation of drops for high-speed microfluidic sorting devices". In: *Applied Physics Letters* 88.2 (2006), p. 024104.

[6] Q. Zhang et al. "Towards high-throughput microfluidic Raman-activated cell sorting". In: *Analyst* 140.18 (2015), pp. 6163–6174.

[7] C. Wilhelm and F. Gazeau. "Universal cell labelling with anionic magnetic nanoparticles". In: *Biomaterials* 29.22 (2008), pp. 3161–3174.

[8] R. Pethig. "Review article dielectrophoresis: Status of the theory". In: *Biomicrofluidics* 4.2 (2010), p. 022811.

[9] Y. Xia and G. M. Whitesides. "Soft lithography". In: *Annual review of materials science* 28.1 (1998), pp. 153–184.

[10] W.-C. Tian and E. Finehout. "Introduction to microfluidics". In: *Microfluidics for biological applications*. Springer, 2008, pp. 1–34.

[11] W. H. Grover et al. "Monolithic membrane valves and diaphragm pumps for practical large-scale integration into glass microfluidic devices". In: *Sensors and Actuators B: Chemical* 89.3 (2003), pp. 315–323.

[12] J. N. Lee, C. Park, and G. M. Whitesides. "Solvent compatibility of poly (dimethylsiloxane)-based microfluidic devices". In: *Analytical chemistry* 75.23 (2003), pp. 6544–6554.

[13] N. Stankova et al. “Optical properties of polydimethylsiloxane (PDMS) during nanosecond laser processing”. In: *Applied Surface Science* 374 (2016), pp. 96–103.

[14] A. Ofner et al. “High-throughput step emulsification for the production of functional materials using a glass microfluidic device”. In: *Macromolecular chemistry and physics* 218.2 (2017), p. 1600472.

[15] C. S. Effenhauser et al. “High-speed separation of antisense oligonucleotides on a micromachined capillary electrophoresis device”. In: *Analytical Chemistry* 66.18 (1994), pp. 2949–2953.

[16] K. Takahashi et al. “Non-destructive on-chip cell sorting system with real-time microscopic image processing”. In: *Journal of nanobiotechnology* 2.1 (2004), p. 5.

[17] R. S. Thomas et al. “Image-based sorting and negative dielectrophoresis for high purity cell and particle separation”. In: *Electrophoresis* 40.20 (2019), pp. 2718–2727.

[18] A. Sciambi and A. R. Abate. “Accurate microfluidic sorting of droplets at 30 kHz”. In: *Lab on a Chip* 15.1 (2015), pp. 47–51.

[19] J. Borovský. “Development of microfluidics for sorting of carbon nanotubes”. In: *Research report/Department of Physics, University of Jyväskylä* 2018, 11 (2018).

[20] J. F. Edd et al. “Microfluidic concentration and separation of circulating tumor cell clusters from large blood volumes”. In: *Lab on a Chip* (2020).

[21] H. Bruus. *Theoretical microfluidics*. Vol. 18. Oxford university press Oxford, 2008.

[22] C. P. Toseland. “Fluorescent labeling and modification of proteins”. In: *Journal of chemical biology* 6.3 (2013), pp. 85–95.

[23] O. Warburg, F. Wind, and E. Negelein. “The metabolism of tumors in the body”. In: *The Journal of general physiology* 8.6 (1927), p. 519.

[24] H. Cai and F. Peng. “2-NBDG fluorescence imaging of hypermetabolic circulating tumor cells in mouse xenograft model of breast cancer”. In: *Journal of fluorescence* 23.1 (2013), pp. 213–220.

[25] H. Shafiee et al. “Contactless dielectrophoresis: a new technique for cell manipulation”. In: *Biomedical microdevices* 11.5 (2009), p. 997.

[26] H. A. Pohl. “The motion and precipitation of suspensoids in divergent electric fields”. In: *Journal of Applied Physics* 22.7 (1951), pp. 869–871.

[27] A. Castellanos et al. “Electrohydrodynamics and dielectrophoresis in microsystems: scaling laws”. In: *Journal of Physics D: Applied Physics* 36.20 (2003), p. 2584.

[28] T. Z. Jubery, S. K. Srivastava, and P. Dutta. “Dielectrophoretic separation of bioparticles in microdevices: A review”. In: *Electrophoresis* 35.5 (2014), pp. 691–713.

[29] M. Li et al. “A review of microfabrication techniques and dielectrophoretic microdevices for particle manipulation and separation”. In: *Journal of Physics D: Applied Physics* 47.6 (2014), p. 063001.

[30] J. Cottet et al. “MyDEP: a new computational tool for dielectric modeling of particles and cells”. In: *Biophysical journal* 116.1 (2019), pp. 12–18.

[31] H. Morgan et al. “Single cell dielectric spectroscopy”. In: *Journal of Physics D: Applied Physics* 40.1 (2006), p. 61.

[32] B. Çetin and D. Li. “Dielectrophoresis in microfluidics technology”. In: *Electrophoresis* 32.18 (2011), pp. 2410–2427.

[33] C. Zhang et al. “Dielectrophoresis for manipulation of micro/nano particles in microfluidic systems”. In: *Analytical and bioanalytical chemistry* 396.1 (2010), pp. 401–420.

[34] R. Pashley et al. “De-gassed water is a better cleaning agent”. In: *The Journal of Physical Chemistry B* 109.3 (2005), pp. 1231–1238.

[35] L. Wu, L.-Y. Lanry Yung, and K.-M. Lim. “Dielectrophoretic capture voltage spectrum for measurement of dielectric properties and separation of cancer cells”. In: *Biomicrofluidics* 6.1 (2012), p. 014113.

[36] K. H. Kang et al. “Continuous separation of microparticles by size with Direct current-dielectrophoresis”. In: *Electrophoresis* 27.3 (2006), pp. 694–702.

[37] F. F. Becker et al. “Separation of human breast cancer cells from blood by differential dielectric affinity”. In: *Proceedings of the National Academy of Sciences* 92.3 (1995), pp. 860–864.

[38] C. F. Ivory and S. K. Srivastava. “Direct current dielectrophoretic simulation of proteins using an array of circular insulating posts”. In: *Electrophoresis* 32.17 (2011), pp. 2323–2330.

[39] S. Franssila. *Introduction to microfabrication*. John Wiley & Sons, 2010.

[40] Moran-Mirabal. *Piranha cleaning - glass surfaces*. 2014. URL: `https://www.chemistry.mcmaster.ca/moran-mirabal/resources/PIRANHA-CLEAN-5-2014.pdf` (visited on 04/10/2020).

[41] J. Klug et al. “Chemical and electrochemical oxidation of silicon surfaces functionalized with APTES: the role of surface roughness in the AuNPs anchoring kinetics”. In: *The Journal of Physical Chemistry C* 117.21 (2013), pp. 11317–11327.

[42] A. Lazauskas and V. Grigaliūnas. “Float glass surface preparation methods for improved chromium film adhesive bonding”. In: *Materials Science* 18.2 (2012), pp. 181–186.

[43] M. Ohring. “Materials science of thin films”. In: *Applied Optics* 31.34 (1992), pp. 95–144.

[44] L. Chen et al. “Study of glass metallization and adhesion evaluation for TGV application”. In: *2013 14th International Conference on Electronic Packaging Technology*. IEEE. 2013, pp. 217–220.

[45] S.-J. J. Lee and N. Sundararajan. *Microfabrication for microfluidics*. Artech house, 2010.

[46] C. Oatley. “The early history of the scanning electron microscope”. In: *Journal of Applied Physics* 53.2 (1982), R1–R13.

[47] “E-Beam Lithography (EBL)”. In: *Encyclopedia of Nanotechnology*. Ed. by B. Bhushan. Dordrecht: Springer Netherlands, 2016, pp. 901–901. DOI: `10.1007/978-94-017-9780-1_100268`.

[48] J. Moore and J. O. Choi. “Degradation of poly (methyl methacrylate) deep UV, X-ray, electron-beam, and proton-beam irradiation”. In: ACS Publications, 1991.

[49] K. R. Williams, K. Gupta, and M. Wasilik. “Etch rates for micromachining processing-Part II”. In: *Journal of microelectromechanical systems* 12.6 (2003), pp. 761–778.

[50] D. Monk, D. Soane, and R. Howe. “A diffusion/chemical reaction model for HE etching of LPCVD phosphosilicate glass sacrificial layers”. In: *Technical Digest IEEE Solid-State Sensor and Actuator Workshop*. IEEE. 1992, pp. 46–49.

[51] C.-H. Lin et al. “A fast prototyping process for fabrication of microfluidic systems on soda-lime glass”. In: *Journal of Micromechanics and Microengineering* 11.6 (2001), p. 726.

[52] W. Guanglong et al. “Microfluidic Chips Etching Process on Soda-lime Glass”. In: *Proceedings of the 1st International Conference on Mechanical Engineering and Material Science*. Atlantis Press. 2012.

[53] C. Iliescu et al. “Characterization of masking layers for deep wet etching of glass in an improved HF/HCl solution”. In: *Surface and Coatings Technology* 198.1-3 (2005), pp. 314–318.

[54] F. E. Tay et al. “Defect-free wet etching through pyrex glass using Cr/Au mask”. In: *Microsystem technologies* 12.10-11 (2006), pp. 935–939.

[55] V. Hägglund. “Characterization of masking layers for deep wet etching in borofloat glass”. In: 2013.

[56] C. Iliescu, B. Chen, and J. Miao. “On the wet etching of Pyrex glass”. In: *Sensors and actuators A: Physical* 143.1 (2008), pp. 154–161.

[57] O. Srivannavit et al. “Design and fabrication of microwell array chips for a solution-based, photogenerated acid-catalyzed parallel oligonuclotide DNA synthesis”. In: *Sensors and Actuators A: Physical* 116.1 (2004), pp. 150–160.

[58] T. Scientific. *Soda-lime microscope slides composition*. 2015. URL: `https://assets.thermofisher.com/TFS-Assets/APD/brochures/objekttraeger_uk_0715_0209.pdf` (visited on 04/21/2020).

[59] H. Park et al. “A review of wet chemical etching of glasses in hydrofluoric acid based solution for thin film silicon solar cell application”. In: *Current Photovoltaic Research* 5.3 (2017), pp. 75–82.

[60] C. Iliescu and F. E. Tay. “Wet etching of glass”. In: *CAS 2005 Proceedings. 2005 International Semiconductor Conference, 2005.* Vol. 1. IEEE. 2005, pp. 35–44.

[61] S. Franssila and L. Sainiemi. “Reactive Ion Etching (RIE)”. In: *Encyclopedia of Microfluidics and Nanofluidics*. Ed. by D. Li. Springer US, 2008, pp. 1772–1781. DOI: 10.1007/978-0-387-48998-8_1344.

[62] T. Plach et al. “Mechanisms for room temperature direct wafer bonding”. In: *Journal of Applied Physics* 113.9 (2013), p. 094905.

[63] M. Poulsen et al. “Towards a microscopic understanding of plasma activated bonding”. In: *Proceedings-Electrochemical Society*. Electrochemical Society. 2003, pp. 248–258.

[64] C. Iliescu et al. “A practical guide for the fabrication of microfluidic devices using glass and silicon”. In: *Biomicrofluidics* 6.1 (2012), p. 016505.

[65] Q. Chen et al. “Thermal assisted direct bonding between structured glasses for lab-on-chip technology”. In: *Microsystem technologies* 15.12 (2009), p. 1873.

[66] Q.-Y. Tong and U. Goesele. *Semiconductor wafer bonding: science and technology*. John Wiley, 1999.

[67] S. Öçal. “Fabrication of microfluidic devices through deep wet etching”. In: (2019).

[68] M. Leman et al. “Droplet-based microfluidics at the femtolitre scale”. In: *Lab on a Chip* 15.3 (2015), pp. 753–765.

[69] M. Bu et al. “A new masking technology for deep glass etching and its microfluidic application”. In: *Sensors and Actuators A: Physical* 115.2-3 (2004), pp. 476–482.

[70] K. T. Tan et al. “Fundamentals of adhesion failure for a model adhesive (PMMA/Glass) joint in humid environments”. In: *The Journal of Adhesion* 84.4 (2008), pp. 339–367.

[71] Y. Huang et al. “Effect of annealing on the characteristics of Au/Cr bilayer films grown on glass”. In: *Vacuum* 71.4 (2003), pp. 523–528.

[72] T. Tisone and J. Drobek. “Diffusion in thin film Ti--Au, Ti--Pd, and Ti--Pt couples”. In: *Journal of Vacuum Science and Technology* 9.1 (1972), pp. 271–275.

[73] L. Tian et al. “A handy liquid metal based non-invasive electrophoretic particle microtrap”. In: *Micromachines* 9.5 (2018), p. 221.

[74] P. Balogh. *Laminar flow of fluorescent microspheres*. 2020. URL: https://youtu.be/Xz-v59IJdyM (visited on 06/30/2020).

[75] P. Balogh. *Fluorescent microspheres flowing to channel corresponding to their lane*. 2020. URL: https://youtu.be/iNh1GMUPQsE (visited on 06/30/2020).

[76] P. Balogh. *Dielectrophoresis testing (failed)*. 2020. URL: https://youtu.be/15CEVs_O_H0 (visited on 06/30/2020).

A Appendix

Table 4. Chemicals information.

Use case	**Name**	**Manufacturer**
Au etching	Gold Etchant, Standard 651818-500ml	Sigma Aldrich
Cr etching	Nichrome etchant 651834-500ml	Sigma Aldrich
Glass etching	Hydrofluoric acid 48%	EMSURE
Glass etching	Hydrochloric acid 37%	AnalaR, NORMAPUR
Piranha solution	Sulfuric acid $95 - 97\%$	EMSURE
Piranha solution	Hydrogen peroxide 30%	AnalaR, NORMAPUR
EBL-resist	PMMA 950K A11	Allresist
EBL-resist (conductive)	Electra 92 (AR-PC 5090)	Allresist

B Appendix, Fabrication recipe

Steps marked with the same colour must be done consecutively during the same day. (Developer1 = MIBK:IPA)

1. (**Drilling**) Drill chip inlets and outlets using a Laser or mechanical drill bits.
2. (**Annealing**) Start with 3-4 chips for time efficiency. Sonicate and scrub with cotton tips in acetone and rinse with IPA. After drying with N_2-gun, put the chips in the furnace within the sample holder. Set Dwelling time 6h on 560°C and make sure there is an N_2 flow within the furnace. When heating and cooling the furnace is set to 4 °C/ min.
3. (**Cleaning**) Take two flat beakers with Acetone and put one on a hotplate to boil. In the cool acetone, scrub chips with cotton tips holding them down with tweezers. Rinse with fresh acetone and put into the boiling one and Sonicate for 2 min. Repeat this step until no visible contamination/dust particles are present when dried with N_2. Then Sonicate in IPA for 1 min and rinse with fresh IPA and put into dH_2O.
4. (**Activation**) Prepare a big and a small beaker filled with dH_2O and a beaker for piranha. Set hotplate to 100 °C. Use acid gloves and metal tweezers! Pour Sulphuric acid (H_2SO_4) FIRST! and then Hydrogen Peroxide (H_2O_2) in a ratio of 3:1. (For a flat beaker 6 ml H_2SO_4 and 2 ml H_2O_2 is enough to cover the chips). Pipet H_2O_2 slowly to avoid a too strong reaction and fast release of gases. Wait until the exothermic reaction has cooled and put it on the hot plate. Dry chips with N_2 and put in piranha for 30 min, lifting them with tweezers from time to time to remove bubbles. Dip chips into dH_2O and rinse under flowing dH_2O properly. Put into beaker with dH_2O. When all chips are rinsed, Put back to piranha for 5 min. When done, wash the chips under flowing dH_2O thoroughly, making sure that no piranha is left in the drilled holes. Contain chips in dH_2O.
5. (**Evaporation, Mask**) Prepare evaporator fully; Clean crucibles and target materials ready, chamber de-vacuumed. In laminar flow room, dry chips with N_2 and put on hot plate 130°C for 2 min to evaporate any moisture on chip surface. Put chips in evaporator (Care! High chance of contaminating chips!). Evaporate 100 nm of Cr with a slow rotation of the substrate.

6. (**Spin-coating**) Properly blow chips with N_2 and put on hotplate 2 min 160°C to remove moisture. Let chip cool on a clean aluminium block and blow with N_2. Place chip in spin coater and turn on suction. Pipette PMMA 950K A4 evenly on the chip, making sure there are no bubbles present. Use pipette to remove possible bubbles. Spin at 3000 rpm for 60 s with a ramp up speed of 500 rpm/s. Postbake on 160°C for 2 min to remove PMMA solvent and cool chip on an aluminium block.

7. (**Exposure, Electrodes**) Scratch PMMA off a small area near where the evaporator holder was, to get the e-beam holder clamp in contact with the metal mask. Otherwise, serious charging and destruction of the resist might occur. You can scratch the mask also to generate "metal dust" that can be used for write field alignment. Set 120 µm aperture with 200 kV, because large areas are to be exposed. The beam current should measure about 10 nA. Use angle correction to align the pattern layout to the chip corners (avoiding any unnecessary exposure). Preform wright field alignment and expose Electrode layout, using a area dose of 215 µC/cm^2. Develop in Developer1 for 40s and then stir in IPA for 10s to stop and flush any developer on the chip. The chips were then Hardbaked at 180°C for 1h.

8. (**Etching**) The mask (100 nm Cr) is etched by submerging the chip in Cr-etchant at 40°C gently shaking for 25s, then dipping and rinsing with dH_2O. Put on HF-protective gear and prepare chemicals and equipment for HF-etch. Pour 18 ml of HF and pipette (glass) 2 ml of HCL and mix them with HF-tweezers. Dip the chip in HF for 2s and stop in dH_2O. Rinse in dH_2O and store chips in fresh dH_2O.

9. (**Cleaning**). An edge of a cleanroom sheet can be used to absorb water from the hydrophobic surface and then dry Gently with N_2. Treat the chips with RIE O_2 clean (60W for 45s) to remove any PMMA contaminants from electrode channels and to reactivate surface. Store chips in dH_2O.

10. (**Evaporation, electrodes**) Prepare evaporator fully; Clean crucibles and target materials ready, chamber de-vacuumed. In laminar flow room, dry chips with N_2 and put on hot plate 130°C for 2 min to evaporate any moisture on chip surface. Put chips in evaporator (Care! High chance of contaminating chips!). Evaporate 10 nm Ti + 50 nm Au + 10 nm Ti + 100 nm SiO_2 with no rotation and 0 angle.

11. (**Lift-off**) Remove PMMA in acetone, Don't sonicate electrodes! Use Cr-etchant to remove the fully remove the mask. Make sure no residues are left in chip where they would matter. If must, sonication and mechanical scrubbing might be applied at the risk of destroying the electrodes.

12. (**Activation, RIE**) Rinse chips with dH_2O and dry with N_2 blowing. Treat chips with RIE O_2 clean (200 W, 2 min, 40 mTorr). Contain chips in dH_2O.

13. (**Evaporation, Mask**) Prepare evaporator fully; Clean crucibles and target materials ready, chamber de-vacuumed. In laminar flow room, dry chips with N_2 and put on hot plate 130°C for 2 min to evaporate any moisture on chip surface. Put chips in evaporator (Care! High chance of contaminating chips!). Using slow rotation at 45° angle, evaporate 50 nm Cr wait 5 min, 200 nm Au, wait 10 min, 100 nm Au. Don't evaporate Au over 1,2 Å/ sec or it will deposit large chunks wasting gold and reducing mask quality.

14. (**Spin-coating**) Properly blow chips with N_2 and put on hotplate 2 min 160°C to remove moisture. Let chip cool on a clean aluminium block and blow with N_2. Place chip in spin coater and turn on suction. Pipette PMMA 950K A11 evenly on the chip, making sure there are no bubbles present. Use pipette to remove possible bubbles. Spin at 3000 rpm for 60s with a ramp up speed of 500 rpm/s. Postbake on 160°C for 3 min to remove PMMA solvent and cool chip on an aluminium block.

15. (**Exposure, Channels**) Same procedure as in step 5. Preform wright field alignment and expose Channel layout, using a area dose of 450 µC/cm^2. Develop in Developer1 for 55s and then stir in IPA for 10s to stop and flush any developer on the chip.

16. (**Etching**) Protect the electrodes by covering them with tape. The mask (50 nm Cr + 200 nm + 100 nm Au) is etched by submerging the chip in Au-etchant for 25s and gently shaking, stop in dH_2O. Next, dip in Cr-etchant for 10s at 40°C gently shaking then dipping and rinsing with dH_2O. Check under microscope, make sure Cr etchant didn't under etch the Au mask by inspecting the chip upside-down under a microscope. Put on HF-protective gear and prepare chemicals and equipment for HF-etch. Pour 18 ml of HF and pipette (glass) 2 ml of HCL and mix them with HF-tweezers. Dip the chip in HF for 55s gently stirring and stop in dH_2O. Rinse in dH_2O and remove PMMA in Acetone. Lift-off Au-mask using hot Cr-etchant. Mechanical help with tweezers should be applied to remove Au-mask. Rinse in dH_2O.

17. (**TDAB**) This step is extremely susceptible to contamination, try to minimize contamination at all means (wear proper face mask etc.). Remember which side of the glass is to be bonded to avoid contaminating it. The chip and the 18×18 mm^2 coverslip is prepared for bonding.

For cover: Take 2x cover glass. Scrub and sonicate (5 min) in hot acetone. Redo with fresh acetone and then rinse and sonicate (1 min) in IPA. Blow dry with N_2. Preform activation as in step 4. Keep to be bonded side upwards. Sonicate in dH_2O for 5 min and put into fresh dH_2O.

For chip with channels: (If "blisters" are present in electrodes, sonication will destroy them!) Rinse and Sonicate upside down (electrodes facing beaker bottom) for 30s in acetone. Rinse and sonicate 10s in IPA. (Sonication time is a trade-off between successful TDAB and destroyed electrodes). Keep in dH_2O until activation. Dry with N_2 and Treat in fresh Room temperature piranha for (7 + 3) min rinsing with dH_2O in between. Keep to be bonded side upwards. Before rinsing put in dH_2O beaker first! Any piranha solution between tweezers and chip can cause it to slip and drop during rinsing! Contain chips in dH_2O.

Rinse the chips in dH_2O and dry with N_2 under laminar flow hood and put them on hotplate 130°C for 2 min in laminar flow room. Cool chips on a clean Al-block. With the help of a tweezer, grab the back of the cover glass and place it on top of the channels-chip. To remove all newton-rings the glasses can be pushed together with your thumb. A force at full strength can be applied, IF the chip is on a completely flat solid surface. If newton rings still remain, or the glasses don't stick together, the whole process step 17 needs to be redone. A properly bonded glass looks as of being one unit. Place the chip cover upwards into the stainless steel holder and put the weight on top. Place the holder in the furnace and set dwell time 585°C for 2h under nitrogen flow.

18.(**Finish**) Lastly, the protective layer (SiO_2) on top of the electrodes will be removed. Treat the chip with RIE Oxide Etch (O2 -flash at 30°C for 4 min (Etches $42\,\mathrm{nm/min}$). This will remove the top layer of protective SiO_2 on the electrode pads and make them conductive.